[AMERICAN JOURNAL OF SCIENCE, VOL. 266, MARCH 1968, P. 129-166]

American Journal of Science

MARCH 1968

GEOLOGIC AND THERMODYNAMIC CHARACTERISTICS OF THE SALTON SEA GEOTHERMAL SYSTEM

HAROLD C. HELGESON

Department of Geology, Northwestern University, Evanston, Illinois 60201

ABSTRACT. The Salton Sea geothermal area lies in a rift valley of the San Andreas fault system in southern California. The geothermal reservoir consists of > 2000 feet of arkosic sand containing interstitial concentrated NaCl-$CaCl_2$-KCl brines. No steam is present underground. The sand is overlain by shale from the surface to a depth of 2000 to 3000 feet. The temperature in the subsurface exceeds 300°C at 3000 feet and 360°C at 7000 feet. Reaction of the geothermal brines with the enclosing sediments has produced epidote-amphibolite metamorphic facies at depths as shallow as 4000 feet. The shale in the upper part of the stratigraphic section acts as an insulator for the sand reservoir. As a result, the temperature-depth profiles below ~ 3000 feet approach adiabatic gradients. The heat flow by conduction in the shale is of the order of 17 x 10^{-6} calories centimeter^{-2} second^{-1}. Thermal convection of pore fluids in the underlying sand appears to be the primary mechanism of heat transfer in the reservoir. The hydrostatic pressure-depth profile in the geothermal area is consistent with a fluid density of one gram centimeter^{-3}. This observation requires the concentration of total dissolved solids in the pore fluids to increase with depth in a proportional relation to the increase in temperature to ~ 3000 feet. In the deeper part of a given well, the salinity of the brine may be constant with increasing depth. The salinity and temperature of the pore fluids decrease outward from the center of the geothermal reservoir. The enthalpy of the brines in the reservoir ranges from 220 to 275 calories gram^{-1}, which is 45 to 90 calories gram^{-1} less than the enthalpy of pure water at equivalent temperatures and pressures. Although the origin of the brines is obscure, it appears likely that they formed by evaporation of Colorado River water originally trapped in the pore spaces of the reservoir sands.

INTRODUCTION

As defined by wells drilled to date (fig. 1), the Salton Sea geothermal area occupies 12 square miles in the vicinity of five small volcanic buttes aligned along the southeastern shore of the Salton Sea. It lies in a region of high heat flow (Von Herzen, 1963; Lee and Uyeda, 1965; Rex, 1966; Wasserburg and others, 1966) and thermal spring activity (Stearns, Stearns, and Waring, 1937; White, 1955; Waring, 1965) which extends along the general trend of the San Andreas fault system in southern California and northwestern Mexico. At present, the only commercial production of geothermal steam for power generation along this trend is that at Cerro Prieto, Mexico, which is approximately 60 miles southeast of the Salton Sea.

Surface manifestations of thermal activity in the vicinity of the Salton Sea are now limited to a few passive CO_2-rich hot springs and a large number of cool mud pots. However, early descriptions of the region indicate that spectacular thermal spring and geyser activity has taken place in the past (LeConte, 1855; Blake, 1855). The thermal springs first attracted commercial interest in 1927 when three exploratory wells were drilled for steam (max depth, 1473 ft). The heat produced by these wells was insufficient to support power generation (Rook and

Williams, 1942). In the 1930's, more than 50 shallow wells (less than 1000 ft deep) were drilled to produce CO_2 for a dry ice plant, but it was not until 1957 when the first deep hole was drilled that large amounts of hot brine were encountered. This "discovery well" (the No. 1 Sinclair) failed as a successful production well, but it sparked renewed exploration for geothermal steam in the Imperial Valley. Twelve geothermal wells have been drilled in the area in the past decade (fig. 1). All of these have been productive except the No. 3 Imperial Irrigation District (IID) well, which was drilled for disposal purposes, and the No. 1 and No. 2 Sinclair wells.

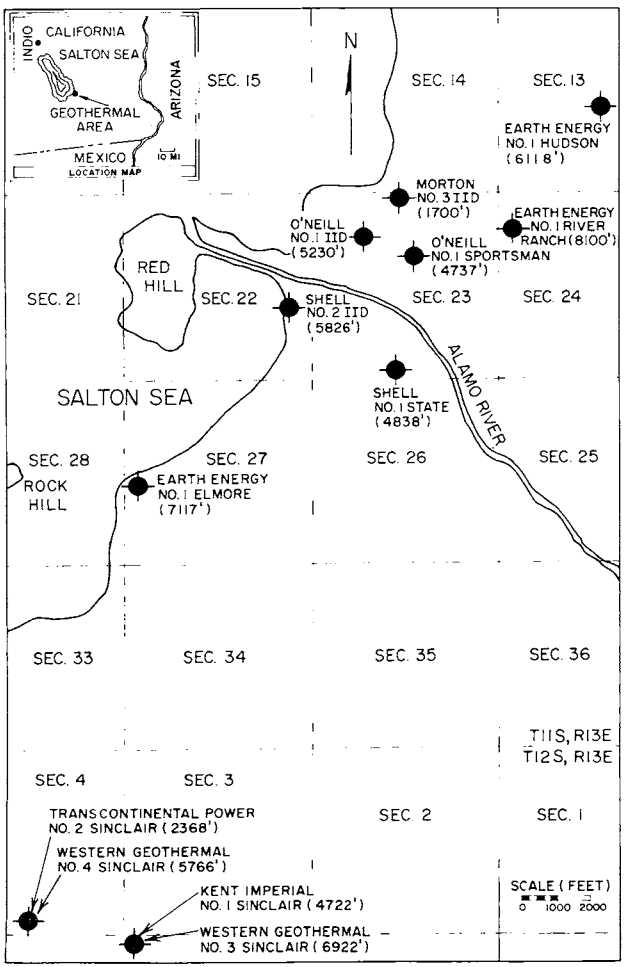

Fig. 1. Map showing well locations in the Salton Sea geothermal area. The shoreline of the Salton Sea fluctuates considerably, and it is therefore not necessarily in the position shown above at the present time. Rock Hill and Red Hill are two of the five volcanic plugs that occur in the vicinity of the geothermal area (see text).

Although similar in certain respects to the geothermal system recently discovered below the Red Sea (Miller and others, 1965; Hunt, Hayes, and Ross, 1967) the Salton Sea geothermal system is unique when compared to most other geothermal areas. Perhaps the most striking difference is the composition of the brines. The brines are rich in sodium, calcium, potassium, and chloride, with relatively large amounts of iron, manganese, silica, strontium, boron, lithium, barium, zinc, lead, copper, and other constituents. Such an exotic composition is not only anomalous with respect to the fluid produced from other geothermal systems, but it is also quite different from the waters issuing from most thermal springs (for example, see Stearns, Stearns, and Waring, 1937; White, 1957a and b; White, Hem, and Waring, 1963). Waters emanating from thermal springs are almost always dilute, and they usually represent deep penetrating ground waters moving through the rocks in response to a pressure differential caused by a thermal anomaly and/or altitude differences between the points of recharge and discharge. In contrast, hot concentrated brines in the Salton Sea geothermal area apparently exist in pressure equilibrium with comparatively cold dilute pore waters in the surrounding rocks. Unlike the geothermal system in Sonoma County, California, no steam is present as a discrete phase in the subsurface; the steam produced in the Salton Sea area flashes from the liquid phase in the flowing wells.

Various aspects of the Salton Sea geothermal system have been discussed by White, Anderson, and Grubbs (1963), White and Muffler (1964), Muffler and White (1965), White (1955, 1963, 1965a, b and c), Craig (1965, 1966), McNitt (1963), Doe, Hedge, and White (1966), Skinner (1963), Skinner and others (1967), Koenig (1967), Berry (1966, 1967), Clayton (1966), Helgeson (1965, 1967a, b), and others. The geology of the region has been summarized by Dibblee (1954) and Longwell (1954), and a number of geophysical investigations have been made by Kelley and Soske (1936), Kovach, Allen, and Press (1962), Biehler, Kovach, and Allen (1964), and others. The present communication is primarily concerned with the subsurface distribution of temperature, pressure, enthalpy, and salinity in the geothermal system. These data are presented in a geological context better to establish the characteristics of the geothermal reservoir.

GEOLOGICAL SUMMARY

Regional setting.—The Imperial Valley consists of a broad flat structural depression filled with lacustrine and deltaic Tertiary sands and shales overlain by Quaternary alluvium. The depression is a rift in the San Andreas fault system which is bordered by mountains of granitic rocks and metasediments underlying a thick Tertiary sedimentary sequence. The major rock units are the Split Mountain (Miocene), Imperial (Upper Miocene-Pliocene), Palm Springs (Pliocene), and Borrego-Brawley (Plio-Pleistocene) formations. Only the Imperial formation contains marine facies. Unlike the Borrego-Brawley formation, which is composed predominantly of shales and siltstones, the Palm Springs is

made up largely of sandstones, often micaceous. The region is highly faulted and structurally complex. It appears to be part of a zone of en-echelon adjustment in the San Andreas fault system along the Banning-Mission Creek, Imperial, San Jacinto, and Elsinore faults.

Marine invasion of the Imperial Valley occurred in Miocene-Pliocene time but only peripherally to the southwest and west of the Salton Sea. Much of the Palm Springs formation to the east and southeast of the Salton Sea is composed of deltaic material derived from the Colorado River. The growth of the Colorado River delta, which began forming in Upper Miocene time, limited contemporaneous sedimentation in this area. The deltaic sediments are greater than 20,000 feet thick (Kovach, Allen, and Press, 1962).

The Salton Sea is a relatively recent phenomenon. Prior to the Colorado River flood of 1905, the depression occupied by the present body of water was nearly dry, but the geologic record indicates that alternate inundation and evaporation has taken place since Miocene time. Evaporites were mined in the late 1800's, and gypsum occurs in occasional veins east of the Salton Sea (and in the mountains to the west), but no significant salt deposits are presently exposed at the surface in the geothermal area.

Stratigraphy and lithology.—The stratigraphy in the immediate Salton Sea geothermal area is relatively simple. A hard, dense shale-siltstone-clay section, probably a facies of the Borrego-Brawley formation, is encountered in the upper parts of the wells. The shale, which contains occasional sand stringers, varies in thickness, but in the center of the geothermal area it is on the order of 2000 to 3000 feet thick. The shale thins considerably to the north, east, and south, but it is believed to thicken under the Salton Sea to the west. In the depth interval between 2000 and 3000 feet the shale becomes more sandy with depth, grading into fine arkosic sand containing intermittent argillaceous intervals. The arkosic sand, which is believed to represent a Colorado River delta facies of the Palm Springs formation, is greater than 2000 feet thick. Below the sand, at depths of 5000 feet or more, a hard, silicified, metamorphosed equivalent (lithologically) of the upper shale-siltstone has been encountered in a number of the wells.

Lithologic changes with depth in two of the geothermal wells are illustrated by the spontaneous potential curves depicted in figure 2. Porosity measurements on core material together with petrographic examination of ditch cuttings and core and sidewall samples indicate that the sand interval between 3000 and >5000 feet (depending on the well) varies from a "tight" quartzitic sand to a sand with porosities of 15 to 20 percent. Although variable, permeabilities in the sand are of the order of 100 millidarcies or less.

Igneous rocks.—Five small rhyolitic plugs intrude the sediments in or near the geothermal area, and sills, dikes, and volcanics have been intersected by the wells. In contrast to the composition of the volcanic plugs, the sills and dikes are porphyritic andesites. The sediments in the

immediate vicinity of the sills and dikes have been subjected to severe chloritic alteration and contact metamorphism. In at least one well, brine is produced from a fracture zone adjoining one of these intrusives. The sills and dikes in the subsurface, as well as the volcanic plugs outcropping along the shore of the Salton Sea, are highly magnetic.

Structure.—Detailed correlation of lithologic and petrophysical logs from well to well in the geothermal area cannot be made with confidence. Although there is little evidence of significant folding or fault movement, open fractures have been intersected by a number of the wells. There is little doubt that these fractures serve as production zones for the wells. However, it is equally apparent (from selective production tests in the wells) that the geothermal brines are derived by the fractures from the pore spaces of the sand reservoir in the immediate geothermal area. At least two sets of fractures have been encountered to date, neither of which has undergone significant displacement. One of these is believed to contribute brine to five wells.

The sedimentary section in the center of the geothermal area is relatively flat; that is, $<15°$ dips. On the flanks, the sediments have a more steeply dipping variable attitude, and to the north, the outcropping beds of the Palm Springs formation are tightly folded.

Geophysical data.—Geophysical investigations by Kovach, Allen, and Press (1962) and Biehler, Kovach, and Allen (1964) indicate the presence of a positive simple Bouguer anomaly over the Salton Sea geothermal area. A positive magnetic anomaly also overlies the area (Kelley and Soske, 1936), and its configuration is roughly coincident with the gravity high. The magnetic anomaly is dominated by the five volcanic plugs aligned along the shore of the Salton Sea, but it also reflects the highly magnetic sills, dikes, and volcanic material in the stratigraphic section. The gravity high is composed primarily of a regional component that becomes increasingly positive from northwest to southeast along the axis of the Imperial Valley, culminating on the southeastern shore of the Salton Sea. When the regional component is removed from the local anomaly, the residual gravity high is consistent with a density contrast of magnitude and extent approximately equivalent to that caused by metasomatic mineralization in the subsurface of the geothermal area. Neither the gravity nor the magnetic anomalies thus necessarily indicate a major intrusive at depth. A seismic profile indicates a depth to "basement" of 19,000 feet about 10 miles to the southwest of the geothermal area (Biehler, Kovach, and Allen, 1964).

Metamorphism.—Phase relations in the geothermal reservoir and changes in the chemical and mineralogic composition of the metamorphosed sediments with depth have been discussed in detail elsewhere (White and Muffler, 1964; Muffler and White, 1965; Helgeson, 1967a). The mineral assemblage in the subsurface consists of K-feldspar + albite (or oligoclase) ± K-mica + chlorite + quartz ± epidote ± calcite between $\sim$ 1500 and 4000 feet. Both primary and secondary quartz, plagioclase, and K-feldspar are present in the assemblage, along with inter-

stitial and vein calcite. Kaolinite and dolomite occur above ~ 1500 feet, and diopside, tremolite, and high-iron biotite appear as metamorphic reaction products below ~ 4000 feet. Pyrite, hematite, quartz, anhydrite, and calcite are commonly encountered in the metamorphosed section. Adularia as well as small amounts of sanidine (adjacent to sills and dikes) have also been identified. Minor quantities of pyrrhotite occur in the reservoir (Skinner and others, 1967) along with sphalerite, galena, and chalcopyrite, but pyrite is the only abundant and pervasive sulfide in the system.

Thermodynamic calculations indicate that reaction of the interstitial brines with the sediments in the geothermal reservoir (which is below ~ 3000 ft) has resulted in substantial mass transfer (> 40 g/1000 g of H_2O) during the metamorphic process (Helgeson, 1967a). However, consideration of the changes in the abundance of metasomatic minerals with depth (fig. 2) suggests that the results of these calculations are minimal. The mineral abundances shown in figure 2 are based on grain counts of heavy mineral fractions separated from ground composite samples of ditch cuttings. On a weight basis, these data indicate that as much as 25 percent of the original sediment has been converted to epidote, pyrite, and hematite in the central part of the geothermal reservoir, and of this, approximately 90 percent is epidote and nearly 10 percent is pyrite. In all the wells, the total abundance of these minerals with depth is approximately proportional to the frequency of sand, as indicated in figure 2. This correlation suggests that the primary porosity in the reservoir rock controlled the extent to which the sediments reacted with the brine in the geothermal system. These reactions have led to partial destruction of the original pore spaces but also to development of secondary porosity. Unlike the primary pores, the secondary pore spaces are poorly connected, which reflects a concomitant decrease in permeability with increasing metamorphism. The contrast in the abundance of the heavy minerals in the two wells in figure 2 reflects the more central position of the Shell No. 2 IID well on the thermal anomaly.

Geochemical and thermodynamic calculations suggest that the reservoir fluids in the geothermal system are in chemical equilibrium with the mineral assemblage in the enclosing rocks, and that the system is essentially closed with respect to the components MgO, CaO, K_2O, Na_2O, Al_2O_3, SiO_2, H_2O, CO_2 and probably also FeO and Fe_2O_3. The fugacities of sulfur, oxygen, and CO_2 vary with temperature (and therefore with depth and position in the reservoir), but at ~ 3000 feet in the No. 2 IID well (where the temp is ~ 300°C), they are of the order of 10^{-10}, 10^{-30}, and 2.5 atmospheres respectively. The composition of the geothermal brines reflects the mineralogic composition of the sediments. Chemical reactions between the original pore fluid in the rock and the sedimentary mineral assemblage has led to a relatively low pH and enrichment of K^+, Ca^{++}, Fe^{++}, and other constituents in the aqueous phase (Helgeson, 1967a). The total dissolved solids in the brine have been concentrated by removal of H_2O from the system.

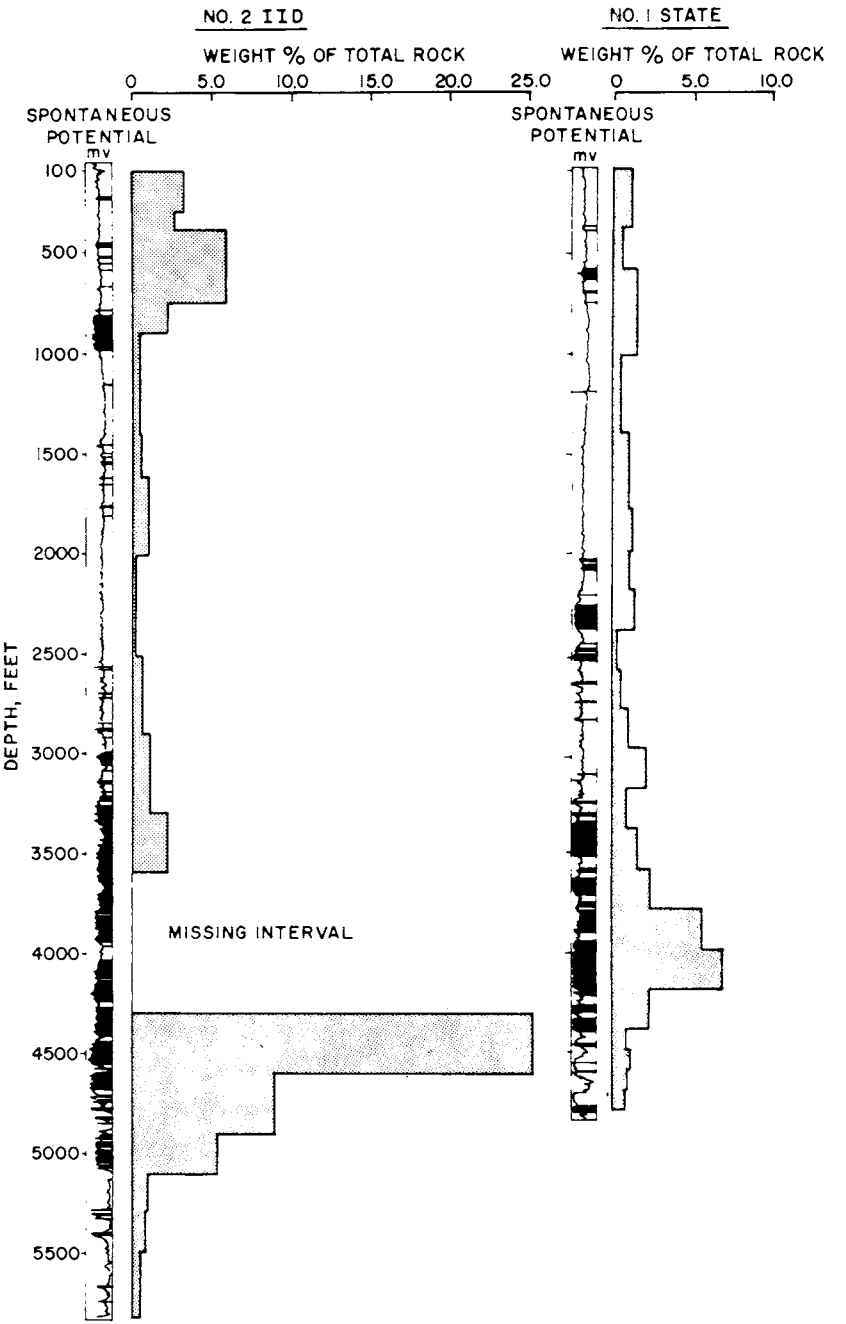

Fig. 2. Total abundance of epidote + pyrite + hematite in the ditch cuttings recovered from the Shell No. 2 IID and No. 1 State wells. The depth distribution of sand encountered in the wells is indicated by the black areas to the right of the spontaneous potential curves.

COMPOSITION OF THE BRINES

Large discrepancies exist among the published analyses of the Salton Sea geothermal brines (White, Anderson, and Grubbs, 1963; White, 1965b; Helgeson, 1965, 1967a). The differences reflect difficulties inherent in obtaining representative samples of the formation fluid from wells producing two-phase flow, as well as various analytical uncertainties caused by the exotic composition of the brines. Of course, real differences in the composition of the brines produced by the various wells from different depths and positions in the reservoir are also reflected in the analyses, but the major discrepancies stem from the fact that White's earlier analyses were not corrected for steam separation (White, Anderson, and Grubbs, 1963; White 1965b); much of this disagreement has since been reconciled (Skinner and others, 1967).

Concentrations of the major constituents of the formation fluid produced from two wells in the geothermal area are listed in table 1. These data have been corrected for steam separation, and they therefore describe the composition of the formation fluid in the geothermal reservoir. The values shown in table 1 are averages of several hundred analyses of (individual) brine, noncondensible, and steam condensate samples from the Shell No. 2 IID and No. 1 State of California wells. These wells produce primarily from perforations at depths of $\sim$ 3650 and 4575 to 4750 feet respectively, where the static temperature is $\sim$ 320°C. However, it will be shown later that comparison of the salinities of the fluids in the producing intervals in these wells under static and flowing conditions indicates that the brines produced by the wells are actually derived from shallower positions in the reservoir than the depths of the producing perforations. As indicated previously, the Shell No. 1 State well occupies a flank position on the thermal anomaly, but the Shell No. 2 IID well is in the center of the anomaly (as presently defined) where high temperatures occur at the shallowest depths.

The composition of the brine in the geothermal reservoir varies with depth and radius in the geothermal system. Total dissolved solids increase from several thousand parts per million at the surface to >250,000 parts per million at 3000 feet in the center of the geothermal area, but the salinity gradients on the flanks of the thermal anomaly are much lower. It will be shown later that the salinity of the brines in the geothermal system is primarily a function of temperature. However, the composition of the brines reflects differences in temperature as well as the mineralogic and chemical composition of the sediments in the various parts of the reservoir.

It can be seen in table 1 that ΣCO_2 in the formation fluid produced by the Shell No. 1 State of California well is an order of magnitude higher than that recovered from the Shell No. 2 IID well. The total number of moles of gas produced per 1000 grams of H_2O in each well is of the same order of magnitude as that produced at Wairakei (5-30 millimoles/100 moles of H_2O; Mahon, 1962). However, the molecular ratio of CO_2 to H_2S produced by the two wells (12 and 120) represents

TABLE 1

Composition (in ppm by weight) of the reservoir fluid produced from the Shell No. 2 Imperial Irrigation District (IID) and Shell No. 1 State of California wells.[a]

Constituent	No. 2 IID	No. 1 State (no inner tubing string) [b]
Sodium	53,000	47,800
Potassium	16,500	14,000
Lithium	210	180
Barium	250	190
Calcium	28,800	21,200
Strontium	440	
Magnesium	10	27
Boron	390	290
Silica	400	
Iron	2,000	1,200
Manganese	1,370	950
Lead	80	80
Zinc	500	500
Copper	3	2
Silver	<1	<1
Rubidium	70	65
Cesium	20	17
Chloride	155,000	127,000
ΣCO_2	500	5,000
ΣS	30	30
Total Dissolved Solids	259,000	219,500

[a] The compositions reported here are for the formation fluid at the depth of production. The numbers are based on material balance calculations involving averages of a large number of brine, noncondensible, and steam condensate analyses together with measured steam qualities (wt percent steam) and ratios of noncondensibles to steam condensate. The analytical work was done by Shell Development Company, Houston, Texas, and the Colorado School of Mines Research Foundation, Golden, Colorado. With the exception of silver and copper, constituents present in trace concentrations have been omitted from the table.

[b] The No. 1 State well was produced with and without an internal 3½-inch tubing string inside the 7⅝-inch casing in the hole. The tubing string, which was 4300 feet long, acted as a downhole choke and changed (reversibly) the performance characteristics of the well. Presumably, different fractures contribute the bulk of the fluid produced by the well, depending on whether the well is equipped with an inner tubing string. These fractures are located at depths of 4575 and 4750 feet.

a larger range than that for CO_2/H_2S produced at Wairakei (15-40; Mahon, 1962). CO_2 accounts for over 90 percent (by volume) of the noncondensibles produced by the wells in the geothermal area; the remainder is composed primarily of H_2S and small amounts of H_2 and hydrocarbon gases.

SUBSURFACE TEMPERATURES

Instruments, procedures, and uncertainties.—Because of the high temperatures in the subsurface, remote recording devices are required to measure temperatures in the geothermal wells. The tools employed for this purpose include Kuster Amerada-type Bourdon tube instruments,

temperature recorders with bimetallic elements, a geothermograph (obtained from Wairakei; Smith, 1958), and maximum recording thermometers of various kinds. These instruments, which have different uncertainty ranges, were run in the wells alternately to check the reproducibility and accuracy of the measurements. Surveys were run at intervals of days, weeks, months, and years in undisturbed wells to document the recovery of the temperature regime from drilling operations and to define any temperature fluctuations in the subsurface. Instruments with clock-driven recorders were hung in various wells to detect and monitor any internal convection occurring in the holes which might obscure the actual formation temperature profile (Donaldson, 1961; Gretner, 1966). Various temperature sensing tools were lowered and raised rapidly, and surveys were run in succession to detect any disturbances caused by the surveys themselves. In all cases, attempts were made to resolve unforeseen ambiguities in the temperature measurements and particularly to evaluate in detail the temperature changes with depth through fracture zones.

As a result of the efforts summarized above it can be concluded that thermal convection in the wells (all of which are completed with $8\frac{5}{8}$-in. or smaller diam casings) and disturbances caused by the surveys themselves have a negligible effect (within the uncertainty of the measurements) on the temperature profiles induced in the wells by the surrounding rock. This is true provided sufficient time is allowed to elapse (> 5 weeks) after completion of a well to permit the temperature regime to recover from disturbances caused by drilling operations. The overall uncertainty range in the results of the surveys is of the order of $\pm 5°C$. No reliable evidence of anomalous temperatures in fracture zones or fluctuations in the temperature profiles with time were detected in the surveys. The conclusions set forth in this paragraph are based on repeated intermittent surveys of the wells from 1963 through mid-1966.

Temperature-depth profiles.—Temperature measurements obtained over a three year period in eight wells in the geothermal area are shown in figures 3 and 4. The temperature-depth profiles defined by the measurements are plotted together in figure 5 for comparison. It can be seen in figure 5 that most of the temperature-depth profiles exhibit a break in slope around 3000 feet, which is the approximate depth at which the lithology changes from shale to sand. The correspondence of the change in temperature gradient and lithology with depth can be seen in the case of the No. 2 IID and No. 1 State wells by comparing the temperature-depth profiles for the wells in figure 5 with their respective spontaneous potential-depth curves in figure 2. The high temperature gradients in the wells above $\sim$ 3000 feet result from heat transfer by conduction in the shale. In contrast to this, the low temperature gradients at depth apparently result from heat transfer by convection in the reservoir sands. The shallow temperature gradients in the No. 3 Sinclair and No. 1 River Ranch wells in figure 5 are not as high as those in the other wells. This can be attributed to the absence or sandy character of the shale in these wells, which are located on the flanks of the thermal anomaly.

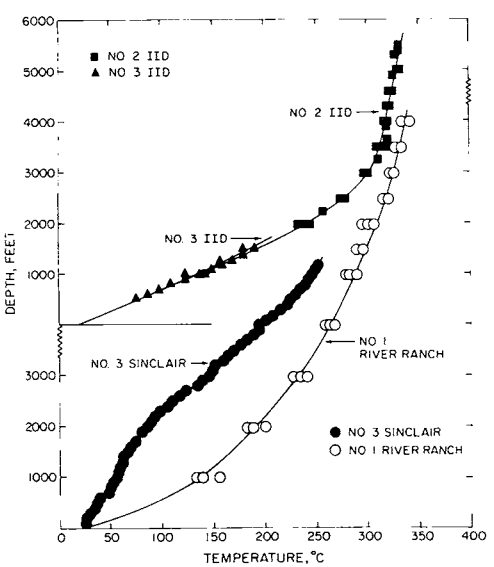

Fig. 3.

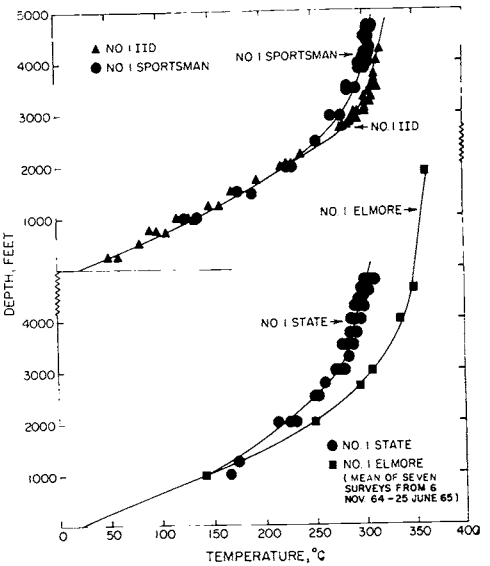

Fig. 4.

Fig. 3. Static temperature-depth profiles in four wells in the geothermal area. The symbols represent temperature measurements obtained intermittently in the undisturbed wells from November 1963 through August 1966.

Fig. 4. Static temperature-depth profiles in four wells in the geothermal area. The symbols represent temperature measurements obtained intermittently in the undisturbed wells from November 1963 through August 1966.

It can be seen in figure 5 that all the temperature-depth profiles are monotonic. No temperature reversals or time fluctuations were detected in the temperature measurements that might reflect subsurface movement of hotter or cooler fluids through the sands or fractures intersected by the wells. This was true in static wells, even when a neighboring well (as close as 1200 ft away) was producing at a high flow rate. Production of fluid from one or more wells, even over prolonged periods, had no effect on the temperature-depth profiles in the surrounding static wells.

The temperature-depth profiles in figure 5 can be used to construct isothermal depth contours on a map of the geothermal area by interpolating linearly between the various wells. Such contours are shown in figure 6 for a 300°C surface. Comparison of these contours with those shown for the gravity and magnetic anomalies in figure 6 indicates that the general configurations of the thermal and geophysical anomalies are approximately coincident. It will be shown below that the isothermal depth contour for 3000 feet in figure 6 is also a curve of constant salinity (275,000 ppm total dissolved solids) of the pore fluids. Isosalinity and isothermal depth contours are also equivalent above 3000 feet, but heat transfer calculations (presented in later pages) indicate that below 3000 to 4000 feet the salinity of the reservoir fluids in a given well may be constant with increasing depth.

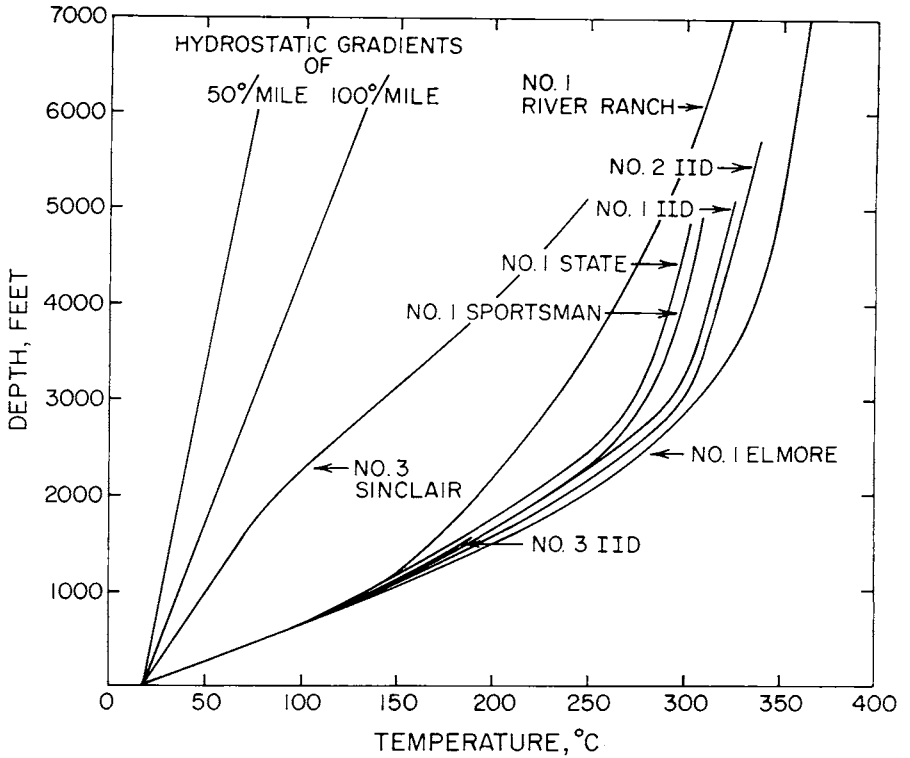

Fig. 5. Composite plot of the temperature-depth profiles defined by the measurements plotted in figures 3 and 4 for eight wells in the geothermal area.

PRESSURE-SALINITY-DEPTH RELATIONS

Pressures measured at casing perforations in various wells in the geothermal area are plotted against depth in figure 7. The measurements were made under static conditions over a period of 3 years with remote recording Amerada-type Bourdon tube instruments calibrated at 260° and 310° C. Within the uncertainty of the measurements (±1.5 atms), all the measured pressures fall on a curve with a 0.0295 atmosphere foot^{-1} gradient, which is a "normal" hydrostatic gradient for the upper crust. This gradient requires the geothermal brines to have essentially unit density at all depths (to at least 7000 ft), which suggests that the hot concentrated brines are in pressure equilibrium with the cold dilute pore waters in the surrounding sediments. The pressure profile in figure 7 permits salinity-depth profiles to be calculated for the various wells.

The relation of salinity to temperature for the geothermal brine along a unit isochore is plotted in figure 8. The curve in figure 8 is based on interpolation of density measurements in a simulated Salton Sea geothermal brine ($KCl : CaCl_2 : NaCl = 1 : 1.95 : 3.55$ by wt) with salinities of 70,000 to 280,000 parts per million at temperatures from 25° to

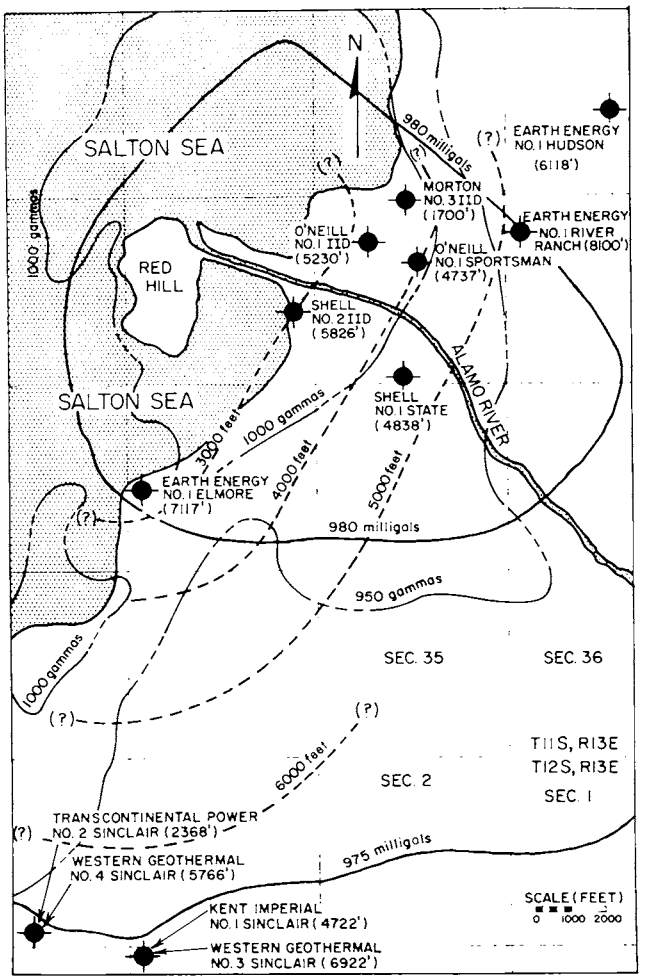

Fig. 6. Map of the Salton Sea geothermal area showing gravity contours (———), magnetic contours (— - - - —), and isothermal-depth contours for a 300°C surface (- - - - -) in the geothermal system. The shaded portion of the map designates the area covered by the Salton Sea. The geophysical data were taken from the literature (Kelley and Soske, 1936; Biehler, Kovach, and Allen, 1964), but the isothermal depth contours are based on temperature-pressure measurements in the wells (see text).

260°C (Nevens and Pool, ms); however, it is also equivalent to that defined by experimental data for the system NaCl-H_2O at high temperature (Ellis and Golding, 1963; Ellis, 1966; Lemmlein and Klevtsov, 1961). Varying the pressure in the system over several hundred atmospheres has a small effect (considered negligible in this discussion) on the curve in figure 8. Because the density of the pore fluids in the geothermal system is insensitive to small changes in the ratios of the constituents of the brine, the curve in figure 8 is a close approximation to the subsurface

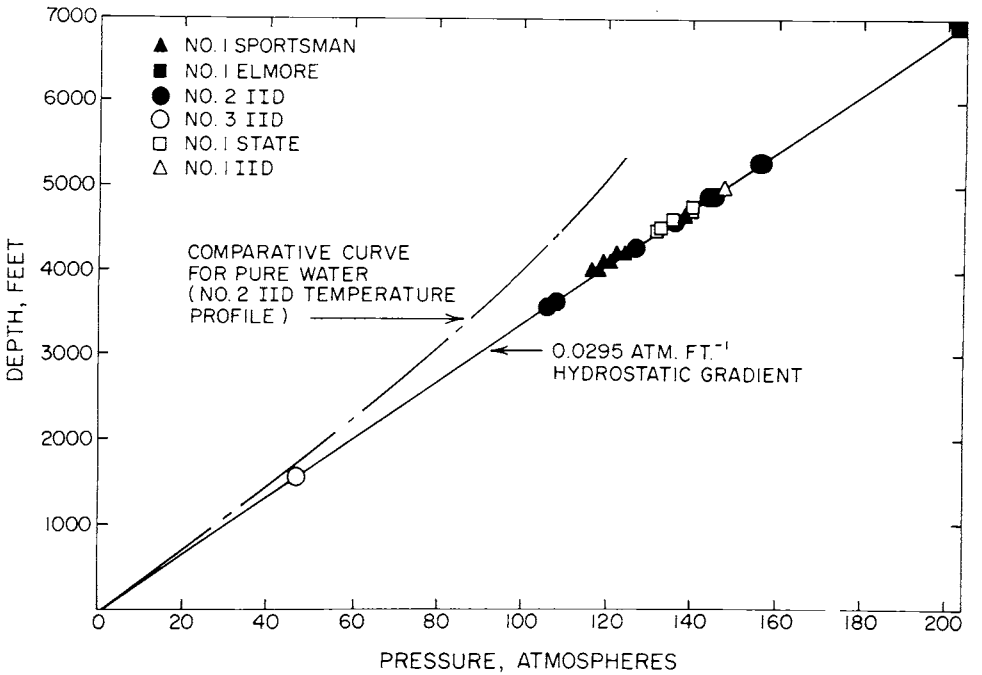

Fig. 7. Pressure measurements at casing perforations in six geothermal wells.

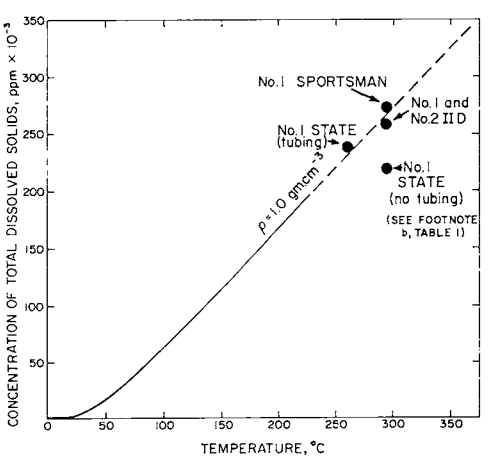

Fig. 8. Dependence of salinity on temperature along a unit isochore for a simulated geothermal brine in the system KCl-$CaCl_2$-NaCl-H_2O (KCl : $CaCl_2$: NaCl = 1 : 1.95 : 3.55 by wt) based on data taken from Nevens and Pool (ms). The solid symbols represent bubble-point salinities and temperatures. The bubble-point salinities were computed from equation (1) and the data shown in figure 14 using a conversion factor of 0.596 ppm total halides per ppm total dissolved solids (see text). The bubble-point temperature for the No. 1 IID well is a measured temperature, but those for the other wells are based on steam quality extrapolations (see text and figs. 13 and 16).

salinity-temperature relation in the geothermal area. This can be seen by comparing the experimental curve with the symbols representing the bubble-points[1] in the various wells. The symbols shown in figure 8 were plotted from data obtained in the wells, all of which produce brines with slightly different ratios of KCl to $CaCl_2$ to NaCl. The fact that the point for the No. 1 State well without tubing in the hole (see footnote [b], table 1) does not fall on the experimental curve is consistent with the higher enthalpy (and lower density) of the fluid entering the perforations in this well when an inner tubing string is not present inside the well casing. The anomalous behavior of the No. 1 State well is discussed further below.

Static salinity-depth profiles are shown in figure 9 for eight wells in the geothermal area. These curves were calculated from the temperature-depth profiles in figure 5 and the temperature-salinity curve in figure 8. It can be seen in figure 8 that the dependence of salinity on temperature along a unit isochore for the geothermal brines is linear above 100°C; consequently, the salinity-depth profiles in figure 9 have the same configurations as the temperature-depth profiles in figure 5.

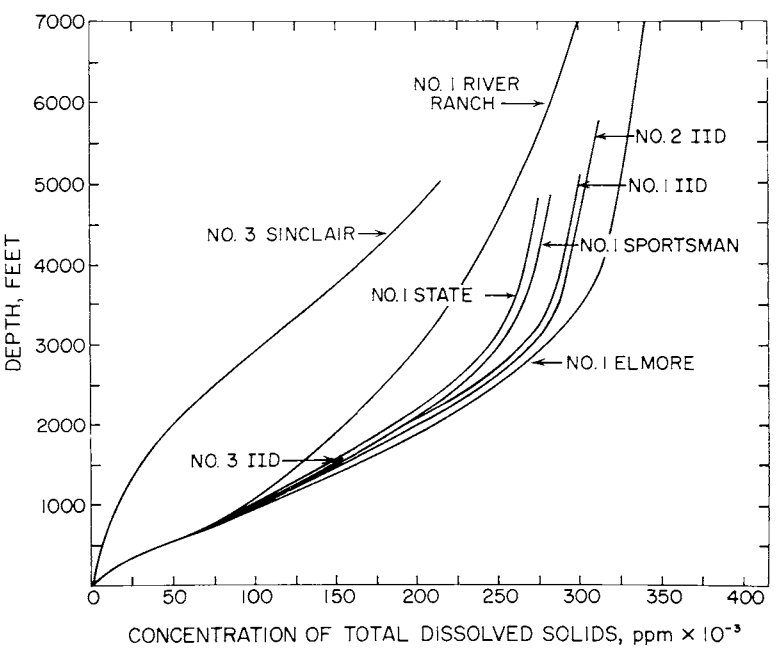

Fig. 9. Calculated salinity-depth profiles for the geothermal wells assuming constant unit density of the subsurface fluids. The curves were computed from the temperature-depth profiles in figure 5 and the temperature-salinity curve in figure 8. Although the curves for the deeper portions of the wells exhibit salinity gradients, the actual profiles below 3000 to 4000 feet may in fact be vertical (see text).

[1] The term "bubble-point" refers to the pressure and temperature at which boiling first occurs as liquid brine rises in a well during production

Because the temperature gradients are low in the deeper parts of the wells, and the uncertainty in the pressure measurements in figure 7 is ~1.5 atmospheres, the slopes of the curves below 3000 to 4000 feet in figure 9 are highly uncertain. Above this depth range the curves must be essentially correct to satisfy the observed pressures[2], but in the deeper parts of the wells the profiles should be regarded only as reference curves for later discussion. It will be shown later that the pressure measurements are not sufficiently accurate to distinguish between an isosaline hydrostatic gradient and an isochoric gradient for unit density (and increasing salinity with depth) below 3000 to 4000 feet. Heat transfer considerations suggest that the true salinity-depth profiles for the fluid in the reservoir sands below the shale are curves of constant or near-constant salinity, which is consistent with a slight decrease in density ($\sim -1.4 \times 10^{-5}$ g cm^{-3} ft^{-1}) with increasing depth below ~3000 feet.

The salinities of fluids produced by the Salton Sea geothermal wells are lower than the computed salinities for the depths of the producing perforations. This can be demonstrated by plotting in figure 9 the salinity of the mass flow produced by a given well against the corresponding depth of the producing perforations. The decrease in bottom-hole salinity in a flowing well is an expected consequence of fracture delivery of brine to the well casing. The depth in the sand reservoir from which the fluid is derived depends on the permeability of the perforated interval and the drawdown pressure in the well during production. In all but the No. 3 IID well, the producing perforations are below 3500 feet. It will be shown later that the temperatures at the producing perforations in the flowing wells are also lower than the static temperatures at equivalent depths. These observations indicate that the fluid produced by a given well is derived from shallower depths than the producing perforations in the well. It appears likely that the brine is derived by fractures from pore spaces distributed over a substantial depth range above the producing perforations. It will be shown in later pages that the decrease in the temperature at the perforations during production of a given well is in part (to the extent of 6°C or less for the drawdown pressures exhibited by these wells) a function of isenthalpic flow and the relative heat capacity of the brine. The role of the relative heat capacity of the brine is reflected by the fact that the slopes of the isenthalps for the brine system on a pressure-temperature diagram are substantially less positive than those of equivalent isenthalps for H_2O. The thermodynamic implications of the salinity-depth profiles and the effect of uncertainties in the slopes of the profiles in the deeper parts of the wells on predictions of the distribution of heat in the geothermal system will be discussed further in later pages.

[2] This observation is true as long as no significant hydrodynamic fluid flow is taking place in the subsurface. No evidence of such flow has been detected in the wells.

RESERVOIR PRODUCTIVITY

A few well performance curves that illustrate the high productivities of the wells in the Salton Sea geothermal area are shown in figures 10 and 11. No change in enthalpy, temperature, or brine composition has occurred during sustained (as long as 18-month) production tests of

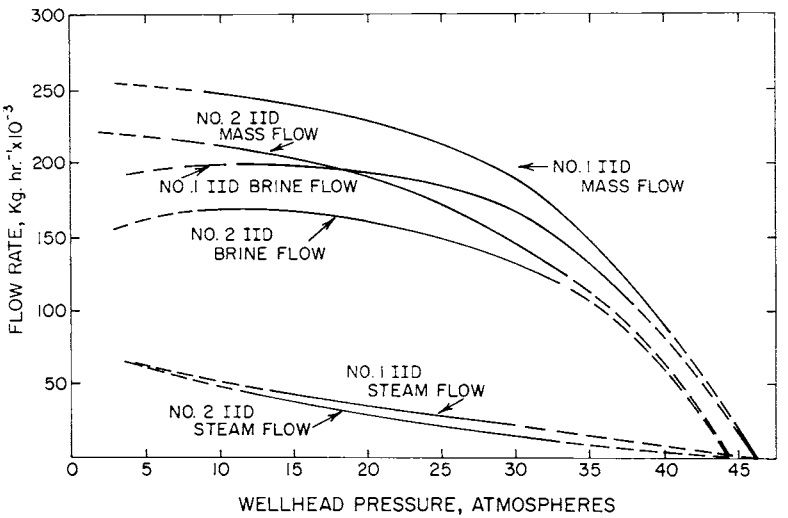

Fig. 10. Flow rate as a function of wellhead pressure in two geothermal wells.

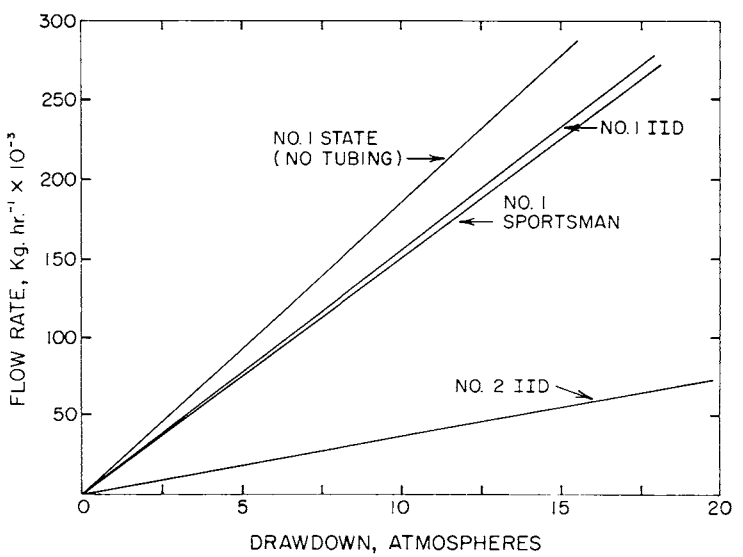

Fig. 11. Flow rate as a function of bottom-hole drawdown (P_{static}-$P_{flowing}$) in four geothermal wells.

the various wells, and no evidence of well interference has been detected. Conservative calculations indicate the presence of more than 5 x 10^{10} feet^3 of concentrated brine and 10^{15} kilocalories of heat (contained in the brine) in the reservoir. With a casing on the order of ten inches in diameter, a single well in the Salton Sea geothermal area is capable of producing more than 350,000 feet^3 of formation fluid per day. In the process, approximately 2700 short tons of dissolved solids and more than 2 x 10^9 kilocalories of heat would be delivered daily to the surface.

ENTHALPY OF THE BRINES

Flow in a highly productive geothermal steam well is essentially adiabatic. Heat transfer calculations indicate that under steady-state conditions less than 2 percent of the heat contained in the brine entering the well perforations is lost to the surrounding rock as the fluid flows to the surface. Because the pressure at a given depth in one of these wells is constant under steady-state conditions, expansion of the fluid in the flowing well is not only adiabatic, it is also isenthalpic.

Owing to the large number of components in the formation fluid, the high temperatures in the reservoir, and the limitations imposed by the data available, only provisional approximations of the enthalpy of the geothermal brines can be calculated in the present state of knowledge. Even this requires an indirect approach. With the exception of saturated salt systems, few thermodynamic data are available for concentrated brines at elevated temperatures, and the pertinent calorimetric data that exist have large uncertainties.

Method of Calculation. — In the following discussion, the concentrations of total dissolved solids (salinity) and (or) total halides (calculated as chloride) are employed as compositional variables. These variables are used to examine the effects of increasing or decreasing salinity on the thermodynamic behavior of the system when the ratios of the constituents in the brines are held constant. Meaningful calculations can be made on this basis because the ratios of the major constituents in the brines do not vary substantially from place to place in the central part of the geothermal reservoir. Sufficient data are not available to evaluate the consequences of compositional variation involving different salts contained in the brine.

Experimental enthalpy-concentration data are plotted in figure 12A for a solution with a fixed KCl : $CaCl_2$: NaCl ratio of 1 : 1.95 : 3.55 (by wt) in equilibrium with its vapor phase in the system NaCl-$CaCl_2$-KCl-H_2O at elevated temperatures (Nevens and Pool, ms). Because of the large experimental uncertainties in the calorimetric data from which the enthalpies were computed, the linear isosalinity curves in figure 12A are only first approximations. However, despite the scatter in the data, these curves are sufficiently accurate up to $\sim$150°C to permit calculation of provisional enthalpies for the Salton Sea geothermal brines. Figure 12B is an enthalpy-concentration cross plot of the curves in figure 12A. For use in later discussion, the isotherms in figure 12B have been extrapo-

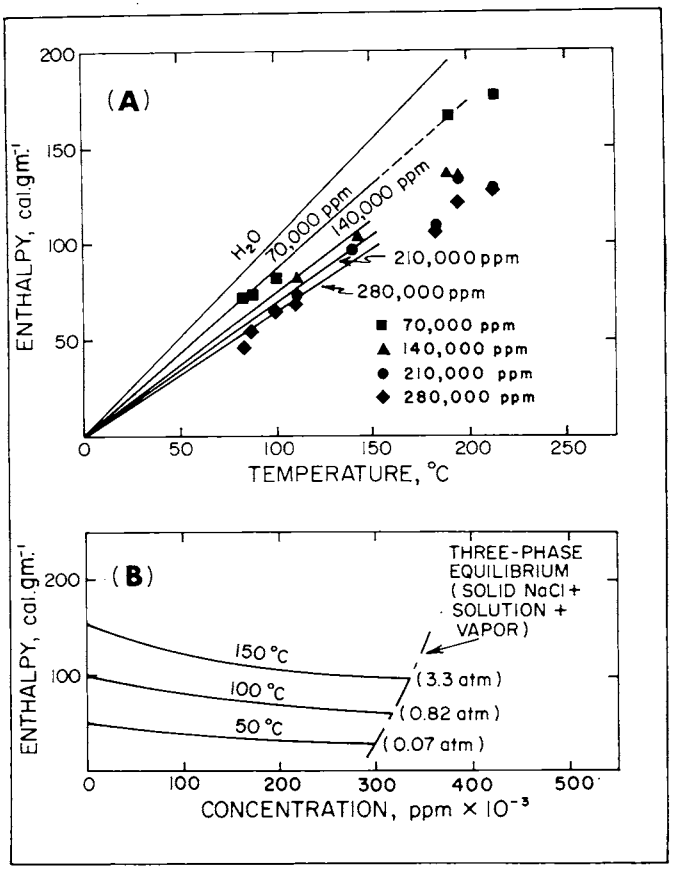

Fig. 12. Enthalpies (relative to 0°C) of a simulated geothermal brine in the system KCl-$CaCl_2$-NaCl-H_2O (KCl : $CaCl_2$: NaCl = 1 : 1.95 : 3.55 by wt) as a function of temperature (A) and concentration (B). The enthalpies are based on experimental data obtained by Nevens and Pool (ms). Figure 12B is a cross plot of the smooth curves in figure 12A. The numbers in figure 12A indicate concentrations of dissolved solids and those in parentheses in figure 12B represent calculated pressures for the intersections of the isotherms with the three-phase equilibrium curve (see text).

lated to the three-phase equilibrium curve (solid NaCl + solution + vapor) defined by experimental solubility measurements at elevated temperatures (Nevens and Pool, ms). Calculated pressures are given in figure 12B for the saturated system. These pressures were computed with the aid of steam tables (Keenan and Keyes, 1936) from measurements of the increase in bubble-point temperature for the simulated geothermal brine over that for pure water as a function of concentration and temperature (Nevens and Pool, ms).

To minimize the effect of uncertainties in the experimental data and those inherent in the pressure-temperature measurements in the flowing wells, the dependence of the enthalpy of the liquid phase on con-

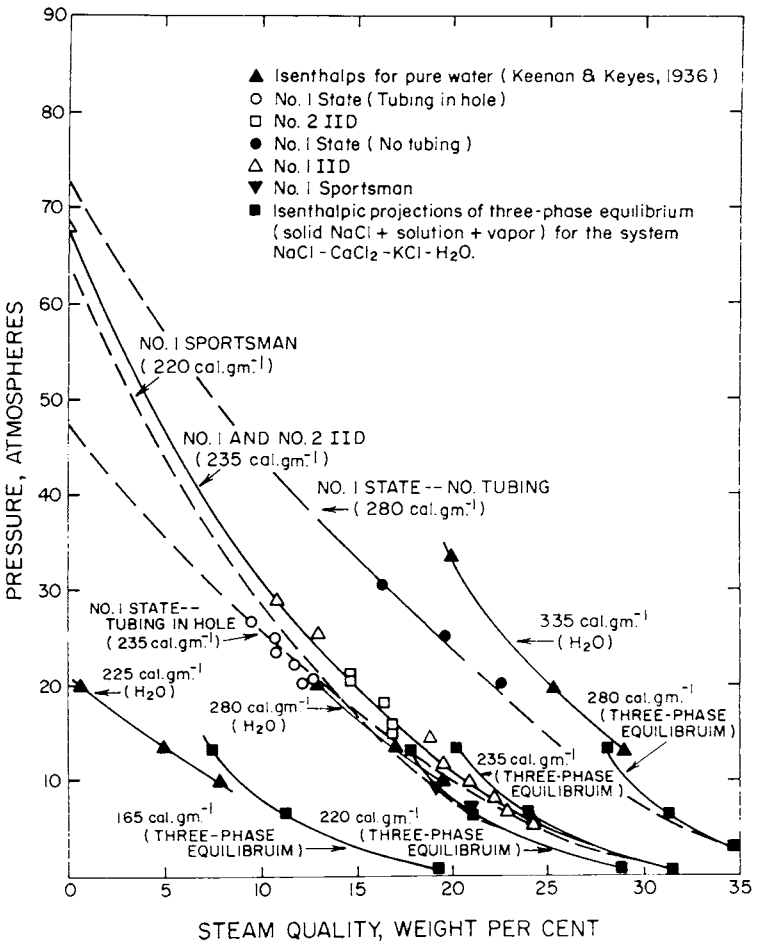

Fig. 13. Abridged steam quality-pressure diagram for the geothermal wells. Comparative curves are shown for pure water (Keenan and Keyes, 1936) along with isenthalpic projections of the three-phase equilibrium for a simulated geothermal brine in the system NaCl-KCl-$CaCl_2$-H_2O (KCl : $CaCl_2$: NaCl = 1 : 1.95 : 3.55 by wt) measured by Nevens and Pool (ms).

centration and pressure along the three-phase equilibrium (fig. 12B) was used to calculate the enthalpy of the geothermal brines. These calculations combine steam qualities (wt percent steam; fig. 13) computed from measurements of brine and steam flow rates with the analytical concentrations of total halides in the brine at given separator pressures. The material balance relation employed in the calculations is

$$C_f = C_b \left(1 - \frac{Q}{100}\right) \qquad (1)$$

in which Q is the steam quality and C_f and C_b represent, respectively, the concentration of total halides in the formation fluid and the con-

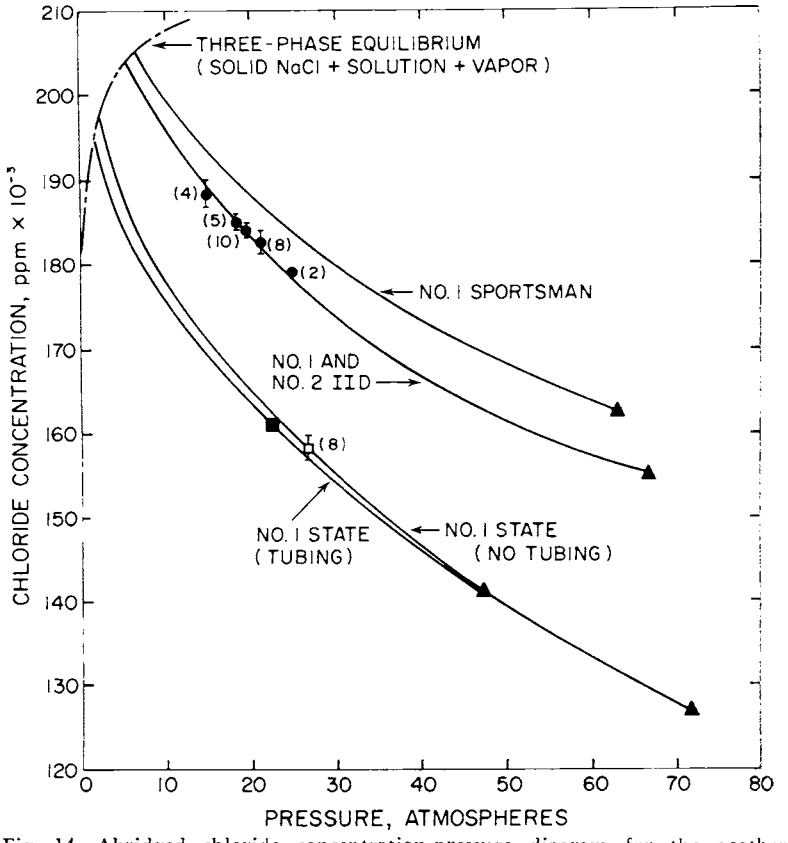

Fig. 14. Abridged chloride concentration-pressure diagram for the geothermal brines. The solid curves represent boiling paths defined by the steam quality curves plotted in Figure 13 and the analytical data represented by the round and square symbols plotted above. The numbers in parentheses indicate the number of samples analyzed and the vertical bars depict uncertainty ranges for the analyses. The triangular symbols represent computed salinities for the bubble-points in the wells. The three-phase equilibrium curve is based on experimental solubility data for a simulated geothermal brine in the system KCl-NaCl-$CaCl_2$-H_2O (KCl : $CaCl_2$: NaCl = 1 : 1.95 : 3.55 by wt) obtained by Nevens and Pool (ms).

centration in the brine after flashing. Having defined a value of C_f for each well, equation (1) can be rearranged to define the two-phase boiling curves for the flowing wells in terms of total halide concentration and pressure. These curves are shown in figure 14 along with the analytical data from which they were calculated.

The curves and bubble-point pressures depicted in figure 14 were computed from the steam quality-pressure curves in figure 13. Although considerable extrapolation is involved in most of these latter curves, it will be apparent in later discussion that the uncertainties introduced by the extrapolations are limited to a considerable degree by the requirement for internal consistency in the thermodynamic behavior of the

geothermal system as reflected by the various wells. The uncertainty in the calculated enthalpies arising from the extrapolations is on the order of ± 5 calories gram^{-1}; however, that arising from ambiguities in the flow measurements and analytical data for the No. 1 Sportsman well is closer to 15 or 20 calories gram^{-1}.

The intersections of the two-phase boiling paths with the three-phase equilibrium curve in figure 14 define the mass flow enthalpies for isenthalpic flow in the various wells. These enthalpies were calculated for each intersection by evaluating

$$H_i = H_b + Q(H_s - H_b)/100 \qquad (2)$$

in which H_i is the enthalpy per unit mass along the isenthalp for the total mass flow, and H_b and H_s are the enthalpies per unit mass of the liquid and steam respectively. The values of H_b used in the calculations were obtained from a cross plot of pressure against enthalpy for the liquid phase along the three-phase equilibrium curve using the values shown in figure 12B. Total halide concentrations were converted to corresponding concentrations of total dissolved solids by assuming a weight ratio of 0.596. This figure was chosen to represent the range of composition (excepting CO_2) exhibited by the geothermal brines produced from the various wells. Because the enthalpy of steam flashing from brine is less than 5 calories gram^{-1} greater than that of steam flashing from pure water at pressures of one to seven atmospheres, and because the solubilities of salts in steam at low pressures and temperatures are exceedingly small, enthalpies for pure steam in equilibrium with water (Keenan and Keyes, 1936) were used in the calculations. After defining values of H_i for each well, values of H_b were computed for higher pressures by rearranging equation (2).

Results. — The enthalpies computed in the manner described above are plotted in figure 15. The isotherms shown in the two-phase region of the enthalpy-pressure diagram in figure 15 are based on pressure-temperature measurements obtained in the flowing wells (fig. 16). Isosalinity curves have been omitted in figure 15 for the sake of clarity.

Although the enthalpy "envelopes" depicted in figure 15 were constructed indirectly and are based in part on extrapolations of data, uncertainties in the calculated enthalpies of the reservoir fluid produced by the various wells are remarkably limited. Even if a substantial error is made in extrapolating a given steam quality curve to low pressures in figure 13, the resulting error in the calculated enthalpy of the mass flow is small. This is true because the slopes of the steam quality curves are similar to those of the isenthalpic projections of the three-phase equilibrium surface[3]. The small variation in the enthalpy of the liquid phase with concentration at low pressures along the three-phase equili-

[3] The three-phase equilibrium projections shown in figure 13 are not strictly isenthalpic because the bulk composition of the system changes along the curves and a heat loss attends precipitation of NaCl. However, this heat loss is less than 2 calories gram^{-1} over the temperature range of interest here.

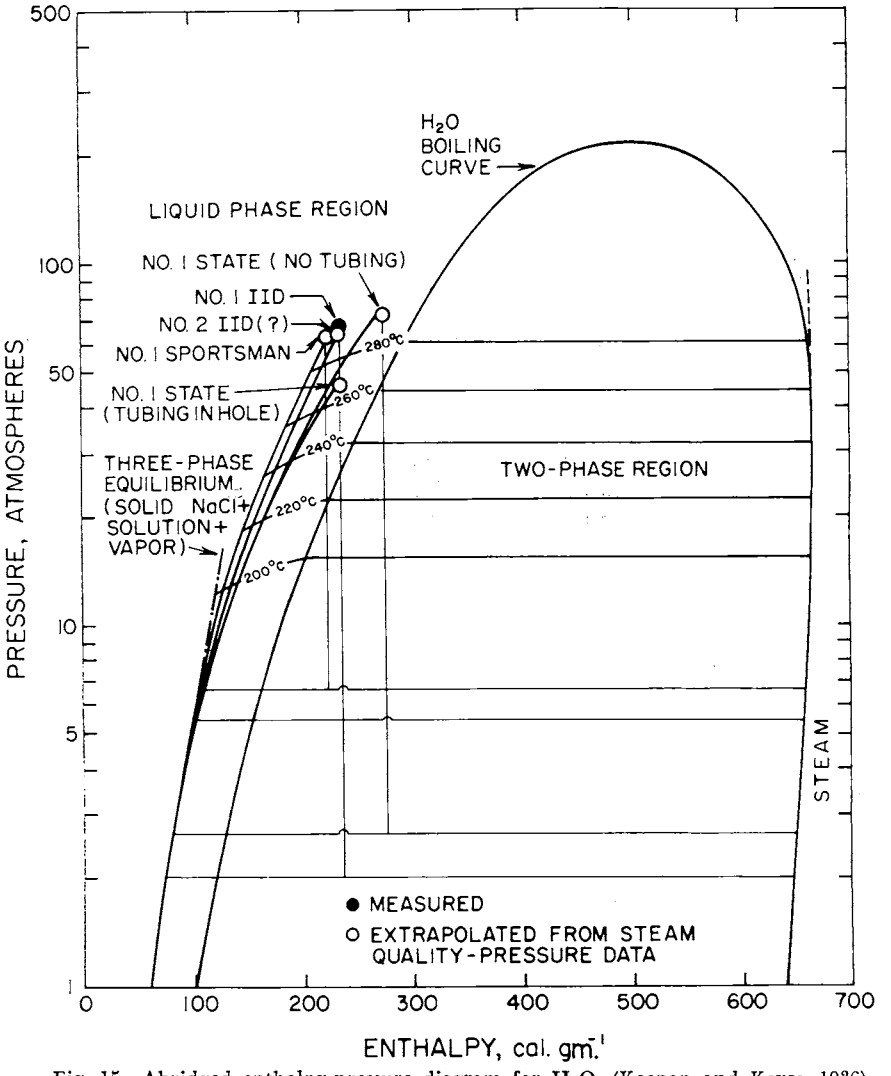

Fig. 15. Abridged enthalpy-pressure diagram for H_2O (Keenan and Keyes, 1936) and the geothermal fluid produced by the wells. The curves shown for the geothermal system were computed from the enthalpy data in figure 12 (see text). The symbols represent the bubble-points (solid = measured, and open = extrapolated) in the wells.

brium also helps to minimize the uncertainties involved in the calculations. On the other hand, because few data are available for the No. 1 Sportsman well, this well may in fact perform like the No. 1 and No. 2 IID wells with respect to temperature, pressure, composition, and enthalpy.

Figure 15 indicates that a high salt concentration in the reservoir fluid causes a decrease in enthalpy of up to 90 calories gram^{-1} from that

of pure water at equivalent temperatures. The heat capacity of the concentrated brine is essentially constant at temperatures up to ~200°C, but it increases rapidly at higher temperatures. At higher temperatures, the enthalpy of the concentrated brine decreases to a much larger extent with increasing concentration than it does at low temperatures. The relative heat capacity of the brine appears to minimize with increasing concentration at high temperatures; as a consequence, if isotherms for 200°C and higher were plotted in figure 12B, they would have negative second derivatives. The relative enthalpy and pressure-temperature-salinity relations for the brine system at elevated temperatures agree qualitatively with what would be predicted from theoretical consideration of high temperature osmotic coefficients for NaCl (Gardner, Jones, and de Nordwall, 1963; Helgeson, 1967a).

PRESSURE-TEMPERATURE-COMPOSITION DIAGRAMS

Pressures and temperatures measured in the flowing geothermal steam wells are plotted in figure 16. The curves defined by these measurements and those obtained at the surface during production tests of the wells are plotted in figure 17, along with various other curves discussed below.

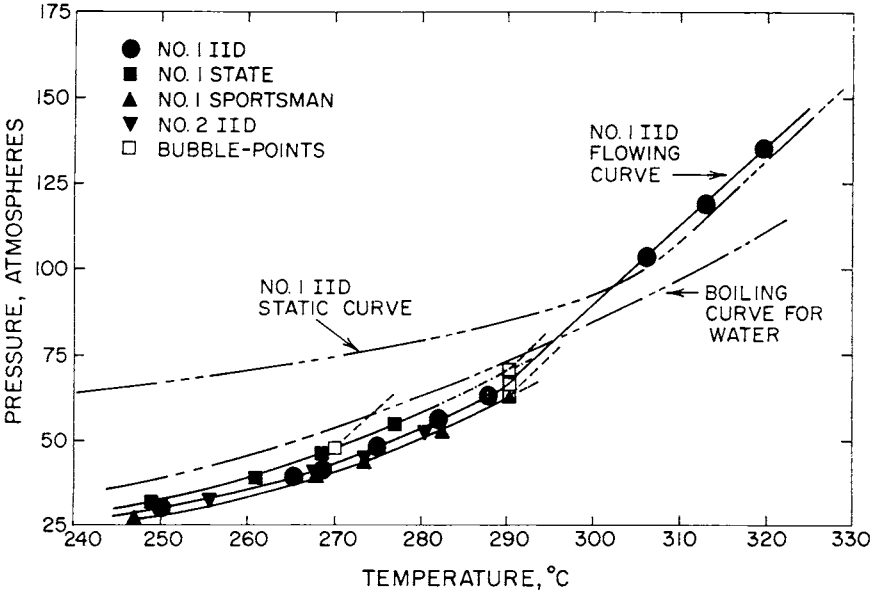

Fig. 16. Measured pressures and temperatures in four flowing geothermal wells. The low pressure curves are boiling paths, but the linear part of the curve for the No. 1 IID well at higher pressures is an isenthalp for liquid phase flow in that well. Except for the No. 1 IID well, open squares designate bubble-points assessed on the basis of extrapolated pressure-temperature-steam quality data (see text). The open square at 270°C on the curve for the No. 1 State well represents the bubble-point for that well with tubing in the hole (see table 1, footnote [b]).

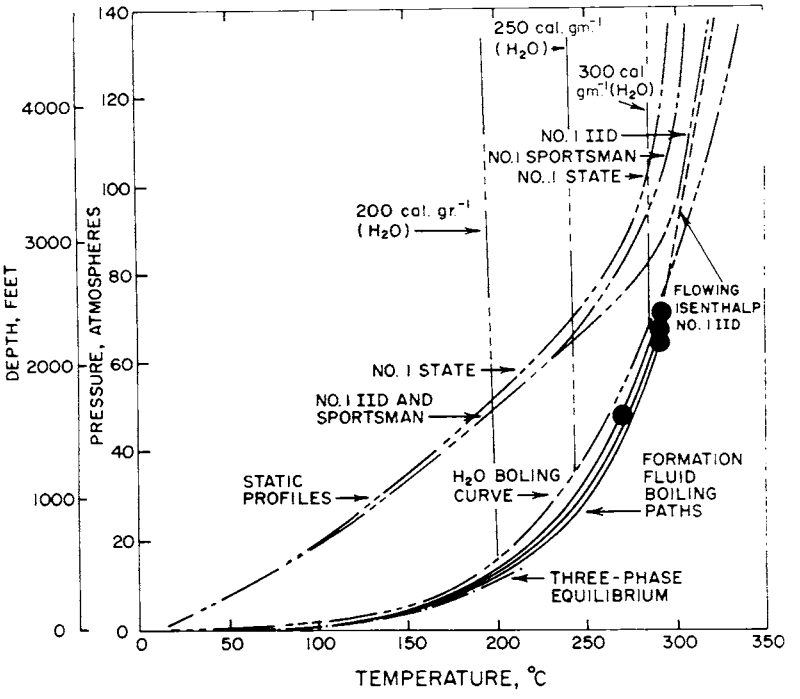

Fig. 17. Pressure-temperature diagram illustrating boiling curves for water (— - - - —) and the fluid produced by the geothermal wells (——), isenthalps for liquid-phase flow in the No. 1 IID well (- - -), static temperature-pressure profiles for the wells (— - - —), the three-phase equilibrium (solid NaCl + solution + vapor) for the geothermal system (— . —), and isenthalps for pure water (— - - - - —). The symbols represent the bubble-points in the respective wells (see fig. 16).

Temperature-composition and pressure-composition diagrams for the brine system are plotted in figures 18 and 19. In each of these diagrams, two additional variables have been superimposed and alternately projected from a third orthogonal axis to the plane of the paper. The dependence of the enthalpy of the liquid phase in the two-phase region on chloride concentration and temperature (fig. 18) or chloride composition and pressure (fig. 19) is illustrated in the diagrams by the family of isenthalpic curves projected to the plane of the paper. If the isenthalps are ignored, corresponding vapor pressures, temperatures, and chloride concentrations in the two-phase region can be assessed for the liquid phase in either diagram.

The dependence of vapor pressure on temperature and chloride concentration depicted in figures 18 and 19 for the liquid phase in the two-phase region of the geothermal brine system is similar to that in the system NaCl-H_2O at higher temperatures (Sourirajan and Kennedy, 1962). The three-phase equilibrium curves for solid NaCl + liquid + vapor in figures 18 and 19 depict the path of the saturated liquid phase

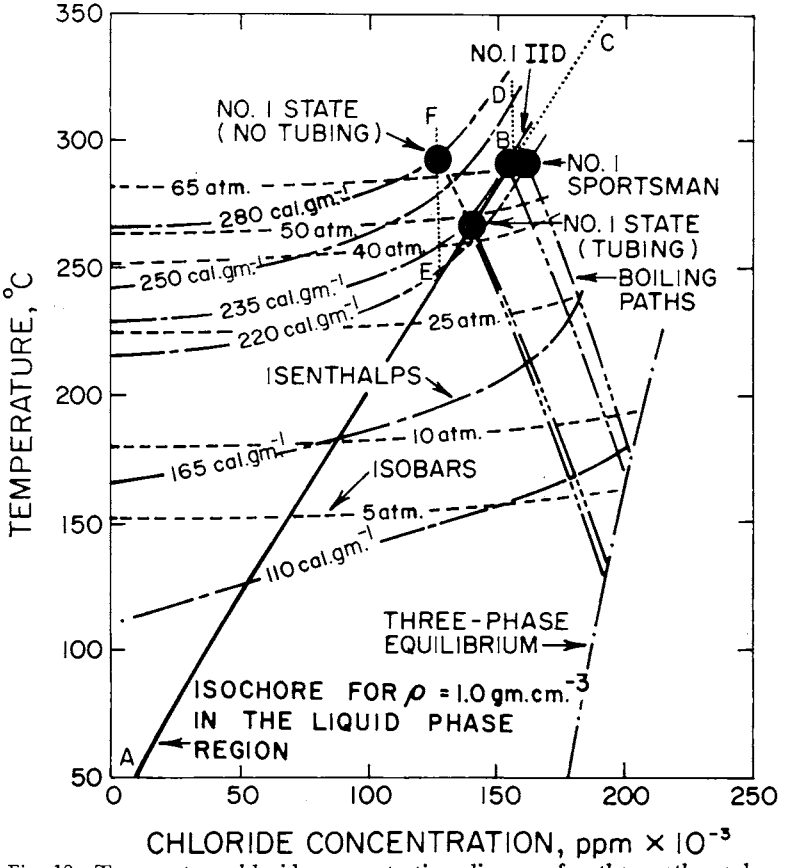

Fig. 18. Temperature-chloride concentration diagram for the geothermal system illustrating isenthalpic (— · —), isobaric (— — —), and polyenthalpic-polybaric (— · · · —) projections for the liquid-phase in the two-phase region. The data for pure water were taken from Keenan and Keyes (1936), and those for the three-phase equilibrium from Nevens and Pool (ms). Line AEB represents the salinity-temperature relation in the liquid-phase region plotted in figure 8, and the dotted curves designate alternate extensions of curve AEB for the geothermal reservoir. The dotted curves were drawn alternately assuming constant unit density (BC) or constant salinity (BD and EF) (see text). The symbols represent the bubble-points in the wells.

without regard to the change in bulk composition of the system arising from precipitation of NaCl. Because the solubility of NaCl does not change substantially along this curve (fig. 12B), this simplification has a negligible effect on the relations shown.

HEAT TRANSFER IN THE GEOTHERMAL SYSTEM

Conduction. — A thermal conductivity of 4 x 10^{-3} calories centimeter^{-1} second^{-1} °C^{-1} is probably a reasonable estimate for the shale in the geothermal area. This value, which is typical for shales (Clark, 1966), requires a heat flow of 17 x 10^{-6} calories centimeter^{-2} second^{-1}

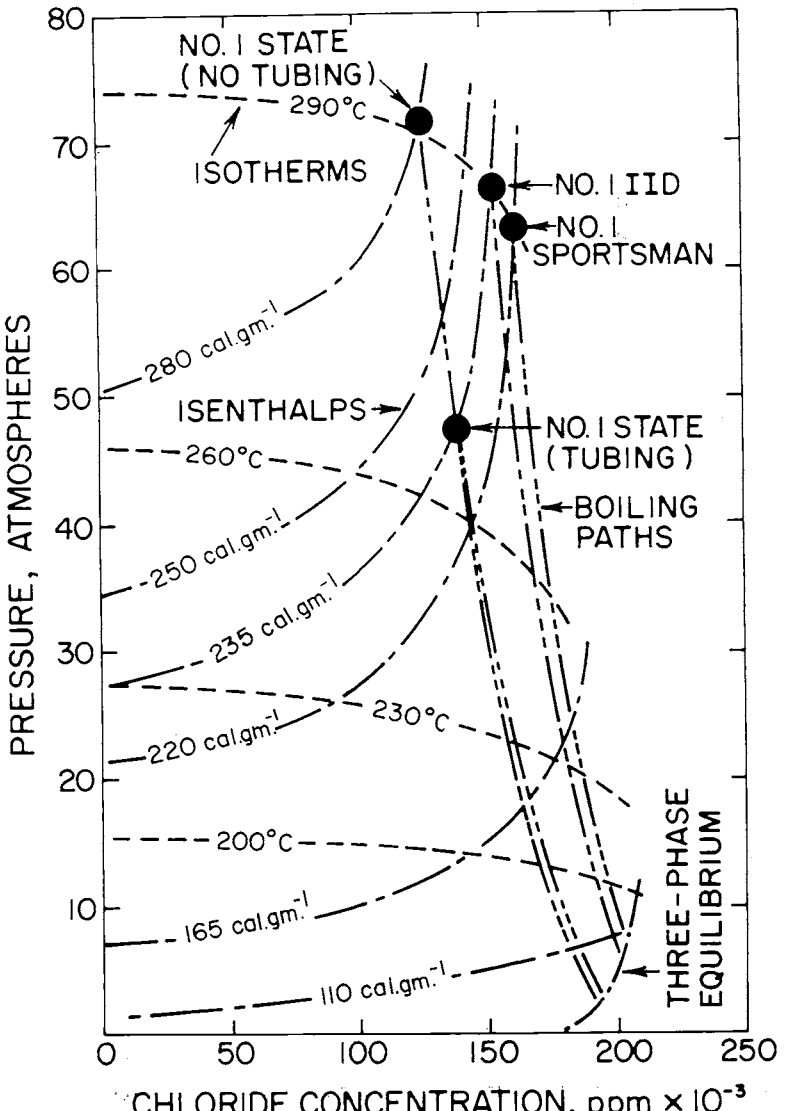

Fig. 19. Pressure-chloride concentration diagram for the geothermal system illustrating isenthalpic (— - —), isothermal (- - -), and polyenthalpic-polythermal (— - - - —) projections for the liquid phase in the two-phase region. The data for pure water were taken from Keenan and Keyes (1936), and those for the three-phase equilibrium curve from Nevens and Pool (ms). The symbols represent the bubble-points in the wells.

to account for the measured temperature gradient (4.2×10^{-3} °C cm^{-1}) in the upper 1000 feet of the stratigraphic section in the center of the geothermal area. If it is assumed (as in the construction of fig. 9) that the pressure measurements in the deeper parts of the geothermal wells

define a hydrostatic gradient exactly consistent with unit density of the pore fluids (0.0295 atm ft^{-1}), free convection is precluded in the geothermal reservoir. On the other hand, in order for heat to be transferred in the reservoir primarily by conduction, the reservoir sand would have to have a thermal conductivity of 39 x 10^{-3} calories $centimeter^{-1}$ $second^{-1}$ $°C^{-1}$ to produce the observed temperature gradient in the reservoir (4.3 x 10^{-4} °C cm^{-1} from 4000 to 5000 ft in the No. 2 IID well). A thermal conductivity of 39 x 10^{-3} calories $centimeter^{-1}$ $second^{-1}$ $°C^{-1}$ is much higher than one could reasonably expect in a sand (Clark, 1966), even when saturated with a concentrated salt solution at high temperatures. Consequently, it appears that convective heat transfer in the reservoir is required to account for the observed temperature-depth profiles, and that the convective density gradient is too small to be defined by the pressure measurements in the static wells. This conclusion is supported by the calculations presented below.

Convection. — The pressure difference between a gravitationally stable column of formation fluid of unit density and a convecting pore fluid of constant salinity in the geothermal reservoir can be computed from experimental densities for the simulated Salton Sea geothermal brine reported by Nevens and Pool (ms). This calculation defines one of several possible limiting conditions for convection in the reservoir.

The density of the reservoir pore fluids at constant composition in the region of 300°C is described by

$$\rho(T) = \rho(T_1) - 10^{-3}(T_2 - T_1) \qquad (3)$$

in which ρ is the density in grams $centimeter^{-3}$ and T represents temperature in °K. Assuming a depth of 3000 feet for the top of the geothermal reservoir, the difference between the pressure that would be caused by a density gradient along a constant salinity temperature-depth profile and the pressure that would result from constant unit density of the pore fluids can be calculated for a depth of 5000 feet in the No. 2 IID well. For this purpose, the temperature gradient (which is essentially constant below ~3000 ft in the No. 2 IID well) can be approximated by adopting an average of 0.014°C $foot^{-1}$ between 3000 and 5000 feet. Equation (3) can now be rewritten as

$$\rho(h) = \rho(h_1) - 14 \times 10^{-6} (h_2 - h_1) \qquad (4)$$

in which h represents depth in feet. Evaluation of equation (4) gives 0.028 grams $centimeter^{-3}$ for the density difference in the brine from 3000 to 5000 feet if the salinity of the brine remains constant over this depth range. The pressure difference (ΔP) between the pressure caused by a unit density profile and that resulting from a linear density gradient in the pore fluids along a constant salinity temperature-depth profile can be calculated from

$$\Delta P(h) = g\rho(h_1)(h_2 - h_1) - g\int_{h_1}^{h_2} \rho(h)dh = \frac{14 \times 10^{-6} g(h_2 - h_1)^2}{2 \times 30.48} \qquad (5)$$

in which g is the acceleration due to gravity.

The pressure difference computed from equation (5) for the depth interval between 3000 and 5000 feet is 0.8 atmospheres. The uncertainty in the measured pressures in the static wells ($\pm$ 1.5 atm) is therefore sufficient to preclude detection of an isosalinity density gradient in the reservoir section of a given well. This is not only true between 3000 and 5000 feet but also from 5000 to 7000 feet. Consequently, although salinity-depth profiles were calculated for the reservoir (and plotted in fig. 9) for a fluid of uniform unit density to 7000 feet, these profiles may in fact be vertical in the deeper parts of the wells. More probably, they are somewhere in between the two extremes. In contrast, the observed temperature gradients in the wells above $\sim$3000 feet are so high that (in the absence of evidence pointing to substantial subsurface flow) the salinity profiles shown in figure 9 for the shallower parts of the wells must be essentially correct to satisfy the pressure profile in figure 7.

The laminar flow velocity of a freely convecting fluid along an isosalinity density gradient is described by Darcy's equation for flow through porous media; that is,

$$v = \frac{K}{\mu}\left(\frac{dP}{dh} - \rho g\right) \tag{6}$$

where v is velocity, K is the permeability of the sand, μ is viscosity, ρ is density, and g is the acceleration of gravity. The value of dP/dh in equation (6) is $0.8/2000 = 4 \times 10^{-4}$ atmospheres foot^{-1}. On the basis of measurements on drill core, the permeability of the sand in the geothermal reservoir is of the order of 100 millidarcies. Substituting these values in equation (6) along with an average density of 0.986 grams centimeter^{-3} and an estimated viscosity of 0.2 centipoises[4] for the geothermal brine yields a flow velocity of 6×10^{-3} centimeters second^{-1}. With a heat content of 235 calories gram^{-1} in the pore fluid (fig. 15), convection would therefore deliver $\sim$1.5 calories centimeter^{-2} second^{-1} to the top of the reservoir ($\sim$3000 ft). However, of the heat delivered, only 17×10^{-6} calories centimeter^{-2} second^{-1} is transferred by conduction to the shale. Although the calculations do not contain provision for heat conduction in the sand or thermal and ionic diffusion leading to the Soret effect (Agar, 1959), it can be shown that these are minor mechanisms of heat and material transfer compared to convection. Nevertheless, it should be stressed that the model examined here is only one of several possible convective mechanisms of heat transfer that may be operating in the reservoir (for example, see Turner and Stommel, 1964).

Speculations on the distribution of heat.—The calculations presented above show that only 0.001 percent of the heat in any given volume of pore fluid convecting in the sand reservoir is transferred to the overlying shale. Under these conditions, the sand reservoir is essentially adiabatic. The sand thus acts as a heat condenser (and exchanger) in the system, with the shale serving as a regulating thermostat. If the sand is truly an

[4] This estimate is based on extrapolated viscosities of sodium chloride solutions at high temperatures (Matthews and Russell, 1967).

adiabatic reservoir, the heat flow from the surface of the geothermal area must equal the heat flow to the sand from below. The nature of the heat source in the geothermal system is unknown. The heat could be supplied from below through deep penetrating fractures that are so far undetected or by conduction through an underlying impermeable rock sequence. The ultimate source of heat may be a cooling intrusive at depth, or the heat may be derived by conduction from the mantle. The latter hypothesis is perhaps more attractive because there is no positive geophysical evidence of a major intrusive at depth, and the crust is abnormally thin (for a continental area) at the southern end of the Imperial Valley (Biehler, Kovach, and Allen, 1964). On the other hand, the presence of plugs, dikes, and sills attests to the occurrence of Plio-Pleistocene volcanism in the immediate geothermal area.

The geometry of the convective system in the geothermal reservoir has yet to be determined. Because fluids with two distinctly different enthalpies have been produced by the wells (220-235 and 275 cal g^{-1}— fig. 15) and because lateral salinity gradients occur in the reservoir; it appears that a number of convection cells are present in the reservoir sands. However, the fact that the hot concentrated brines in the center of the sand reservoir (as presently defined) grade radially to dilute cold pore waters in the surrounding sediments is also consistent with a single convection cell with a central point heat source. If multiple cells exist in the reservoir, their geometry is probably controlled to a certain degree by flow channels associated with dikes, sills, and fractures. Experimental evidence (Elder, 1965) indicates that a broad flat heat source underlying a porous bed with a much larger lateral dimension than vertical thickness gives rise to multiple convection cells.

The relative magnitude of the heat flow in the geothermal area compared to the regional heat flow in the Imperial Valley is not yet well defined. Rex's (1966) data and calculations suggest that the heat flow diminishes quite rapidly to the south but that there are a number of other thermal anomalies in the southern Imperial Valley. Biehler, Kovach, and Allen (1964) interpret their seismic refraction data in terms of a regional pattern of convection cells and local metamorphism in the area southeast of the Salton Sea. It is interesting to note in this regard that a heat flow of 17×10^{-6} calories centimeter^{-2} second^{-1} would require the rock above 2000 feet in the No. 3 Sinclair well (fig. 1) to have a thermal conductivity of 16×10^{-3} calories centimeter^{-1} second^{-1} °C^{-1} in order to satisfy the measured temperature gradient in the upper part of that well (fig. 3). The No. 3 Sinclair well is on the southern flank of the geothermal anomaly (fig. 6) where the shale is thin and sandy. In the present state of knowledge, it appears reasonable that the Salton Sea thermal anomaly is due principally to the presence of shale in an area of abnormally high heat flow. A thick section of shale does not occur elsewhere (except under the Salton Sea) in the southeastern end of the Imperial Valley. In regions of higher than average heat flow such as the Imperial Valley, the presence of an impermeable shale with a low thermal

conductivity allows heat to be stored and high temperatures to build up in underlying sands through geologic time.

Adiabats in the liquid phase region.—Adiabatic (or near adiabatic) convection in the geothermal reservoir is reflected by the steep temperature profiles in the deeper parts of the wells (fig. 5). This can be seen by comparing the static temperature-pressure curve for the No. 1 IID well with the flowing temperature-pressure curve for that well in figures 16 and 17. The low-pressure curves for the flowing wells plotted in figure 16 are boiling paths (along which the salinity of the liquid phase changes) for two-phase flow in the wells. The linear curve for the flowing No. 1 IID well at higher pressures represents isenthalpic-isosaline liquid-phase flow in that well. As indicated previously, this is true in the flowing well because the heat loss to the surrounding rock is negligible and the pressure at any given depth under steady-state flow conditions is constant. Unfortunately, pressure-temperature measurements are not available for the liquid phase region in the other flowing wells. The bubble-point pressure in the No. 1 IID well is defined by the intersection of the isenthalp with the boiling curve in figure 16. It can be seen in figure 17 that this isenthalp has a considerably less positive slope than its pure water equivalent. As plotted, the static pressure-temperature curve for the No. 1 IID well below ~3000 feet in figure 16 coincides almost exactly (within 1°C) with the isenthalpic profile of liquid phase flow in that well. This suggests that the pore fluids in the sand section intersected by the No. 1 IID well are in fact isenthalpic in the reservoir. However, it is shown below that the uncertainty in the temperature measurements is sufficient to preclude a definitive conclusion in this regard solely on the basis of the temperature observations in the wells.

The heavy line labeled AEB in figure 18 represents the temperature-salinity relation required for constant unit density of the pore fluids with depth (fig. 8). Line AEB is thus a projection of superimposed pressure-temperature curves for the static wells lying in a vertical plane with pressure as a third orthogonal axis. Only the characteristics of the liquid phase *in the two-phase region* are shown in the plane of the paper. The dotted extension BC at the high temperature end of AEB is a projection of the unit isochore in the liquid phase region below ~3000 feet. Line BC is thus consistent with the absence of convection in the reservoir. The dotted lines labeled EF and BD are projected curves of constant salinity in the liquid phase region below ~3000 and ~4000 feet respectively, along which the density of the pore fluid changes and convection occurs. Projection of these alternate pressure-temperature profiles (BC, EF, and BD) for the various wells on the pressure-temperature diagram in figure 17 produces almost identical slopes for the curves based on constant density and those calculated for constant salinity at pressures corresponding to a depth of ~3000 feet or more. Of the alternatives, only curves BD, EF, or some intermediate curve between BC and BD (or EF and EB) can be isenthalpic. This is true because the isenthalpic surfaces projected in figure 18 are inclined toward lower salinities and higher temperatures

in the liquid phase region as pressure increases (above the plane of the paper).

Consideration of the phase diagrams in figures 17 and 18 indicates that the difference in slopes between an isosaline-adiabatic and an isochoric-adiabatic temperature-depth profile in the geothermal reservoir cannot be distinguished within the uncertainty ($\pm 5°C$) of the temperature measurements in the wells. Although one of the profiles (that for the No. 1 IID well—fig. 16) appears to be isenthalpic, the evidence for this depends on the accuracy of the curve drawn through the data points for the deeper part of the well (fig. 4). Consequently, it appears that the only definitive conclusion that can be reached in this regard at the present time is that the deep temperature-depth profiles for the various wells appear to approach isenthalpic gradients, and that the salinity and density gradients below $\sim$3000 to 4000 feet are small.

Discussion of the anomalous behavior of the No. 1 State well.—From the relations discussed above it appears that the No. 1 State well (without tubing in the hole—see footnote [b], table 1) produces brine from a portion of the reservoir consistent with a convective path along curve EF in figure 18, where a more dilute brine exists at a given temperature and depth than that in the other wells. Because the brine produced from this source is more dilute for equivalent temperatures than the brine produced by the other wells, it has a higher heat content. The brine produced from this well without tubing in the hole is apparently derived from a deeper source in the reservoir than that produced by the other wells. As indicated previously, consideration of pressure-temperature-salinity relations for the brine system suggests that the other wells derive their fluid from the upper part of the reservoir (in the vicinity of 3000 ft), even though the producing perforations are at deeper depths (>3500 ft, except for the No. 3 IID disposal well). This conclusion is supported by the relations portrayed in figure 17 and the coincidence of the symbols for the wells (other than the No. 1 State well) with the curve for constant unit density in figure 8. In constrast, the fluid produced by the No. 1 State well without tubing in the hole has a density of $\sim$0.97 grams centimeter^{-3} in the reservoir. According to the heat transfer calculations presented above, this density may occur in the reservoir at a depth in the vicinity of 5000 feet where the enthalpy of the brine may be as high as 275 calories gram^{-1}. This would require the temperature profile in that part of the reservoir to be intermediate between the observed profiles for the No. 1 State and No. 1 River Ranch wells in figure 5. Such a profile would require a salinity of about 220,000 parts per million at 3000 feet. If the salinity remained constant with increasing depth, then the characteristics of that part of the reservoir at a depth of 5000 feet would be similar to those exhibited by the flowing No. 1 State well without tubing in the hole. This, however, would require the enthalpy to increase by $\sim$50 calories gram^{-1} along the profile from 3000 to 5000 feet, which implies that the fluid is produced from a different convection cell than the other wells.

The fact that ΣCO_2 produced by the No. 1 State well without tubing in the hole is an order of magnitude higher than that produced by the other wells is consistent with a higher temperature source for the fluid, a lower pH environment, and a partial pressure of CO_2 between 20 and 25 atmospheres. The pH of the brines in the geothermal reservoir is controlled by equilibrium between the mineral assemblage in the rock and the interstitial solution. A source depth of 5000 feet or more for production from this well without tubing in the hole appears reasonable from a geochemical point of view (Helgeson, 1967a). The fluid produced from the No. 1 State well when an inner tubing string is in the hole apparently comes from a shallow part of the reservoir adjacent to the well. The characteristics of the well with tubing in the hole are similar to those of the other wells in the geothermal area, and they are also consistent with the static temperature profile observed in the well.

SPECULATIONS ON THE ORIGIN OF THE GEOTHERMAL BRINES

Various hypotheses have been advanced to explain the origin of the Salton Sea geothermal brines. White and his co-workers (1963) believed originally that the brines were predominantly magmatic in origin. However, White (1965c) has since argued in favor of a meteoric source for the brines. Berry (1966, 1967) has suggested that the brines achieved their high salinities as a result of hyperfiltration of dilute pore waters through semi-permeable shales in the stratigraphic section, and White (1965a) has pointed out chemical similarities of the brines to membrane concentrated connate waters. On isotopic evidence, Craig (1963, 1966) and White (1965c) rule out magmatic water and sea water as possible sources for the geothermal brines. These authors suggest that the brines formed from local rainwater (run-off from the surrounding mountains) that leached NaCl and other salts from the sediments. Their argument is not convincing because it is based on isotopic analyses of relatively few samples, most of which were taken from surface features such as mud pots, warm springs, and shallow CO_2 wells. The fact that the deuterium to hydrogen ratio in these waters is the same as that in the geothermal brine samples does not rule out Colorado River water as a candidate for the fluid responsible for the brines found in the geothermal reservoir.

To support his argument in favor of leaching salts by local ground water, Craig (1966) claims to have documented a linear relation between O^{18}/O^{16} and the logarithm of the chloride concentration in water samples from the Salton Sea geothermal area. However, recent isotopic analyses by Clayton (personal communication) of brine produced from a drill-stem test in the 1550 to 1700 foot depth interval in the No. 3 IID well do not support the dependence of O^{18}/O^{16} on chloride concentration suggested by Craig. Possibly as a result of contamination by drilling fluid[5],

[5]Although isotopic evidence argues against contamination by drilling fluid of the brine produced in the drill-stem test of the No. 3 IID well (Clayton, Muffler, and White, ms), pressure-temperature-density calculations indicate that the salinity of the fluid produced in the test is much too low to be consistent with the observed temperature profile and bottom-hole pressure in the well. In the absence of evidence for a

the brine produced in this drill-stem test was dilute (~35,000 ppm total dissolved solids), but the O^{18}/O^{16} was approximately the same as that in the deep geothermal brines. Assuming a constant O^{18}/O^{16} for the geothermal brines, Clayton, Muffler, and White (ms) have obtained remarkably good agreement between predicted temperatures from isotopic equilibria and those observed in the No. 1 River Ranch well. Although the O^{18}/O^{16} in the brine thus appears to be independent of depth, the data reported here indicate that the chloride concentration in the geothermal brines is a function of temperature and depth in the subsurface, and none of the brines encountered to date has been found to be saturated with respect to NaCl. Other considerations notwithstanding, O^{18}/O^{16} in the geothermal brines would be expected to vary primarily as a function of the reactions taking place between the brines and the mineral assemblages in the sediments.

In general, the various theories of origin discussed above for the reservoir brines are not compatible with the observed temperature-pressure-salinity-enthalpy relations in the geothermal system. On the other hand, these relations are consistent with concentration of the brines by evaporation of dilute pore waters through geologic time. When the deltaic sand sediments containing interstitial Colorado River water were originally subjected to an influx of heat from below, the density of the pore fluids over the heat source must have decreased initially. If permeabilities in the sand section were large enough, this would cause the hot fluids to move upward and the cold surrounding pore fluids to migrate toward the heated area. Assuming that the rising hot fluids over the heat source had access to the surface through fractures or interconnected permeable sand lenses in the shale, evaporation would occur, and the liquid phase would become more saline. If the liquid phase (which would then have a higher density on cooling than the surrounding cold pore waters) circulated back underground, a closed system of recycling pore fluid would be established.

During the process described above the shale acts as a thermal insulator for the system, promoting convection in the underlying sand. Each

---

substantial hydrodynamic pressure in the subsurface, these data require the salinity profile shown for the well in figure 9. Even if the pressure measurement (which has been reproduced in several surveys) shown in figure 7 for the No. 3 IID well is assumed to be in error to the extent of the maximum uncertainty of the measurement, it would not be sufficient to explain 35,000 parts per million total dissolved solids at 1550 feet.

The brines first produced from geothermal steam wells in the Salton Sea area are commonly diluted by water derived from drilling muds. Because the drill-stem test of the No. 3 IID well was short in duration, and because the flow line was a small diameter pipe, production of diluted brine over the period of the test would be anticipated. This is particularly true in the case of the No. 3 IID well because it was drilled without mud; fresh Alamo River water was used for the drilling fluid. If the isotopic evidence precluding contamination of the brine produced in the drill-stem test is accepted, then the brine must have been derived from a shallower depth than 1550 to 1700 feet in order to be consistent with the temperatures and pressure subsequently observed in the static well. A good candidate for a shallow source of production is the relatively thin porous sand that occurs in the geothermal area at depths ranging from 500 to 1000 feet (see fig. 2). Petrophysical evidence in other wells suggests that this sand contains brine with salinities of the order of 25,000 parts per million.

time the brines recirculate to surface, more H_2O is lost, and they become increasingly more saline. In order to maintain hydrostatic equilibrium between the geothermal system and the cold dilute pore waters in the surrounding sediments, the heavier brines would tend to migrate to the deeper (and hotter) parts of the stratigraphic section. However, the convective process in the sand reservoir would tend to homogenize the salinity of the pore fluids in any one convection cell below the shale.

The efficiency of the evaporation process in concentrating the geothermal brines depends on the temperature at the surface. If the temperature were high enough to cause flashing to occur, the buildup of salinity with time could be quite rapid. For example, assuming original dilute pore water containing 1000 parts per million total dissolved solids is transported to the surface and flash evaporated at ~230°C to atmospheric pressure, and assuming the enthalpy of the water to be 235 calories $gram^{-1}$, if the steam is lost to the atmosphere, a given volume of water would have to cycle through the system about 15 times to achieve a salinity greater than 200,000 parts per million. Even with a mean flow velocity as low as 1×10^{-4} centimeters $second^{-1}$ and a cycle distance of 6000 feet, this would take only on the order of 1000 years. If no flashing occurred in the evaporation process, the time involved would be much longer. Flash evaporation of interstitial Colorado River water through geologic time would tend to produce the isotopic characteristics of the geothermal brines reported by Craig (1966).

Waters in most geothermal systems do not become concentrated as a result of flash evaporation in the manner discussed above. Progressive cyclic concentration of the underground waters by flashing at the surface is precluded in these systems because the liquid phase fails to circulate back underground. In most geothermal areas, the post-flash liquid phase joins the surface water run-off. In the Salton Sea geothermal area this is not possible because the area is more than 200 feet below sealevel. From geologic evidence, apparently it has been a base level depression since Miocene times.

An alternate process of concentration by evaporation has been suggested by Hemley (personal communication). This process involves loss of water molecules through semipermeable shales as suggested by Berry (1966, 1967), but the driving mechanism is provided by the heat from below. The limiting condition for the process is the establishment of solvent pressure equilibrium between the hot concentrated brine and the cold dilute pore waters in the surrounding sediments.

In conclusion, the thermodynamic characteristics of the Salton Sea geothermal system appear to be most consistent with an origin of the geothermal brines from lower Colorado River water originally trapped in the deltaic sediments. Salt filtering may have played a role in the evolution of the brines, but evaporative processes appear to be a more likely alternative. Whatever the mechanism, isotopic (Doe, White, and Hedge, 1963; Doe, Hedge, and White, 1966) and geochemical (Helgeson, 1967a) considerations suggest that the chemical composition of the geothermal

brines has been affected to a considerable extent by reactions between the pore fluids and the sediments in the high temperature environment in the subsurface. Ellis and Mahon (1964) have been led to similar conclusions with regard to the Wairakei geothermal system. Although the brines contain only 30 parts per million sulfur (present as H_2S), there is little doubt that they constitute potential ore-forming fluids (Helgeson, 1967b). The bulk of the metals in solution were probably derived from the enclosing sediments, and the thermodynamic and chemical characteristics of the brines, as well as the geothermal system itself, may be representative of those responsible for many hydrothermal ore deposits. The low sulfide, high chloride, and "acid" (Helgeson, 1967a) nature of the brines is perhaps the most significant characteristic in this regard. It is also probably more than coincidental that the geothermal brines are similar in many respects to fluids commonly found in fluid inclusions in hydrothermal minerals.

ACKNOWLEDGMENTS

I am indebted to R. E. Wyman, L. W. Midland, J. C. Taylor, R. Bean, and other members of the staff of Shell Oil Company for their help and cooperation during the course of this study. Investigations by W. Ahr, B. Wilson, G. Edwards, H. E. Gray, and others employed by Shell Development Company contributed substantially to the present understanding of the geothermal system. The efforts of L. Kreisel and C. Smith of Morton Salt Company and R. Dondanville and C. Otte of Earth Energy, Inc. in obtaining data are also acknowledged with thanks. The bulk of the discussion presented in the foregoing pages is based on data collected under the auspices of Shell Oil Company and Morton Salt Company, who released these data for publication. Earth Energy, Inc. and Western Geothermal, Inc. also cooperated in making available temperature data for their wells. Thanks are due R. Roy, P. Goldreich, and others at the California Institute of Technology for their interesting comments and discussion during an oral presentation of this paper in February, 1967. Finally, I would like to express my appreciation to R. C. Speed and R. M. Garrels of Northwestern University, C. L. Christ, J. J. Hemley, D. E. White, and L. J. P. Muffler of the U.S. Geological Survey, and A. J. Ellis of the Department of Scientific and Industrial Research, New Zealand, for their helpful discussions, suggestions, and critical reviews of the manuscript.

REFERENCES

Agar, J. N., 1959, Thermal diffusion and related effects in solutions of electrolytes, *in* Hamer, W. J., ed., The structure of electrolytic solutions: New York, John Wiley & Sons, Inc., p. 200-223.

Berry, F. A., 1966, Proposed origin of subsurface thermal brines, Imperial Valley, California: Am. Assoc. Petroleum Geologists Bull., v. 50, p. 644-645.

———— 1967, Role of membrane hyperfiltration on origin of thermal brines, Imperial Valley, California, [abs.]: Am. Assoc. Petroleum Geologists Bull., v. 51/3, p. 454-455.

Biehler, S., Kovach, R. L., and Allen, C. R., 1964, Geophysical framework of the northern end of the Gulf of California structural province, *in* Marine Geology of the Gulf of California: Am. Assoc. Petroleum Geologists Mem. 3, p. 126-143.

Blake, W. P., 1855, Reports of exploration and surveys for a railroad from the Mississippi River to the Pacific Ocean, 1853-54: Executive Doc. 78, 33rd Cong. [U.S.A.], 2nd Sess.

Clark, S. P., Jr., 1966, Thermal conductivity, *in* Clark S. P., Jr., ed., Handbook of physical constants: Geol. Soc. America Mem. 97, p. 460-482.

Clayton, R. N., 1966, Oxygen isotope exchange in rock-water systems, an abstract: Am. Geophys. Union, v. 47, p. 203.

Clayton, R. N., Muffler, L. J. P., and White, D. E., ms, 1967, Oxygen isotope study of calcite and silicates of the River Ranch well, Salton Sea geothermal area, California.

Craig, H., 1963, The isotopic geochemistry of water and carbon in geothermal areas, *in* Tongiorgi, E., ed., Nuclear geology of geothermal areas: Rome, Consiglio Naz. delle Ricerche, p. 17-53.

———— 1966, Isotopic composition and origin of the Red Sea and Salton Sea geothermal brines: Science, v. 154, p. 1544-1547.

Dibblee, T. W., 1954, Geology of the Imperial Valley Region, California: Calif. Bur. Mines Bull., v. 170, p. 21-28.

Doe, B., Hedge, C. E., and White, D. E., 1966, Preliminary investigation of the source of lead and strontium in deep geothermal brines underlying the Salton Sea geothermal area: Econ. Geology, v. 61, p. 462-483.

Doe, B., White, D. E., and Hedge, C. E., 1963, Preliminary isotopic data for brine and obsidian near Niland, California [abs.]: Mining Eng., v. 15, p. 60.

Donaldson, I. G., 1961, Free convection in a vertical tube with a linear wall temperature gradient: Australian Jour. Physics, v. 14, p. 529-539.

Elder, J. W., 1965, Physical processes in geothermal areas, *in* Lee, W. H. K., ed., Terrestrial heat flow: Am. Geophys. Union, Geophys. Mon. Ser., v. 8, p. 87-190.

Ellis, A. J., 1966, Partial molal volumes of alkali chlorides in aqueous solution to 200°: Jour. Chem. Soc., London, p. 1579-1584.

Ellis, A. J., and Golding, R. M., 1963, The solubility of carbon dioxide above 100°C in water and in sodium chloride solutions: Am. Jour. Sci., v. 261, p. 47-60.

Ellis, A. J., and Mahon, W. A. J., 1964, Natural hydrothermal systems and experimental hot-water/rock interactions: Geochim. et. Cosmochim. Acta, v. 28, p. 1323-1357.

Gardner, E. R., Jones, P. J., and de Nordwall, H. J., 1963, Osmotic coefficients of some aqueous sodium chloride solutions at high temperatures: Faraday Soc. Trans., v. 59, p. 1994-2000.

Gretner, P., 1966, On the thermal stability of large diameter wells, an abstract: Am. Geophys. Union, v. 47, p. 182.

Helgeson, H. C., 1965, High temperature solution chemistry of sulfides, *in* Roedder, Edwin, ed., Report on S.E.G. symposium on the chemistry of the ore-forming fluids: Econ. Geology, v. 60, p. 1380-1403.

———— 1967a, Solution chemistry and metamorphism, *in* Abelson, P. H., ed., Researches in Geochemistry, v. II: New York, John Wiley & Sons, p. 362-404.

———— 1967b, Silicate metamorphism in sediments and the genesis of hydrothermal ore solutions, *in* Brown, J. S., ed., Symposium on the genesis of stratiform lead-zinc-barite-fluorite deposits: Econ. Geology, Mon. 3, p. 333-342.

Hunt, J. M., Hayes, E. E., and Ross, D. A., 1967: Red Sea: detailed survey of hot brine areas: Science, v. 156, p. 514-516.

Keenan, J. H., and Keyes, F. G., 1936, Thermodynamic properties of steam: New York, John Wiley & Sons, 89 p.

Kelley, V. C., and Soske, J. L., 1936, Origin of the Salton volcanic domes, Salton Sea, California: Jour. Geology, v. 44, p. 496-509.

Koenig, J. B., 1967, The Salton-Mexicali geothermal province: Calif. Div. Mines and Geology Mining Inf. Serv., v. 20, no. 7, p. 75-81.

Kovach, R. L., Allen, C. R., and Press, F., 1962, Geophysical investigations in the Colorado Delta Region: Jour. Geophys. Research, v. 67, p. 2845-2871.

LeConte, J. L., 1855, Account of some volcanic springs in the desert of the Colorado in Southern California: Am. Jour. Sci., 2d ser., v. 19, p. 1-6.

Lee, W. H. K., and Uyeda, S., 1965, Review of heat flow data, *in* Lee, H. K., ed., Terrestrial heat flow: Am. Geophys. Union, Geophys. Mon. Series, v. 8, p. 87-190.

Lemmlein, G. G., and Klevtsov, P. V., 1961, Relations among the principal thermodynamic parameters in a part of the system H_2O-NaCl: Geochemistry, v. 2, p. 148-158.

Longwell, C. R., 1954, History of the Lower Colorado River and the Imperial Depression, California: Calif. Bur. Mines Bull., v. 170, p. 53-56.

Mahon, W. A. J., 1962, The carbon dioxide and hydrogen sulfide content of steam from drillholes at Wairakei, New Zealand: New Zealand Jour. Sci., v. 5, p. 85-98.

Matthews, C. S., and Russell, D. G., 1967, Pressure buildup and flow tests in wells: Henry L. Doherty Mon. Ser.: Soc. Petroleum Engineers, v. 1, p. 158.
McNitt, J. R., 1963, Exploration and development of geothermal power in California: Calif. Div. Mines and Geology, Spec. Rept. 75, p. 31-34.
Miller, A. R., Densmore, C. D., Degens, E. T., Hathaway, J. C., Manheim, F. T., McFarlin, P. F., Pocklington, R., and Jokela, A., 1965, Hot brines and recent iron deposits in deeps of the Red Sea: Geochim. et Cosmochim. Acta, v. 30, p. 341-359.
Muffler, L. J. P., and White, D. E., 1965, Recent metamorphism of Pliocene and Quaternary sediments of the Salton Sea geothermal field, California, U. S. A. [abs.]: Internat. Symposium on Volcanology Abs., New Zealand, p. 119-120.
Nevens, T. O., and Pool, M. J., ms., 1964, Determination of thermodynamic properties of brines: Denver Research Inst., Contract Research Rept. 2151 with revisions, 22 p.
Rex, R. W., 1966, Heat flow in the Imperial Valley of California [abs.]: Am. Geophys. Union Trans., v. 47, p. 181.
Rook, S. H., and Williams, G. C., 1942, Imperial carbon dioxide gas field: Calif. Div. Oil and Gas Bull., v. 28, p. 12-23.
Skinner, B. J., 1963, Sulfides deposited in the Salton Sea geothermal brine [abs.]: Mining Eng., v. 15, p. 60.
Skinner, B. J., White, D. E., Rose, H. J., and Mays, R. E., 1967, Sulfides associated with the Salton Sea geothermal brine: Econ. Geology, v. 62, p. 316-330.
Smith, J. H., 1958, Production and utilization of geothermal steam: New Zealand Eng., v. 13, p. 354-375.
Sourirajan, S., and Kennedy, G. C., 1962, The system H_2O-NaCl at elevated temperatures and pressures: Am. Jour. Sci., v. 260, p. 115-141.
Stearns, N. D., Stearns, H. J., and Waring, G. A., 1937, Thermal springs in the United States: U. S. Geol. Survey Water Supply Paper 679-B, 206 p.
Turner, J. S., and Stommel, H., 1964, A new case of convection in the presence of combined vertical salinity and temperature gradients: Natl. Acad. Sci. Proc., v. 52, p. 49-53.
Von Herzen, R. P., 1963, Geothermal heat flow in the Gulfs of California and Aden: Science, v. 140, p. 1207-1208.
Waring, G. A., 1965, Thermal springs of the United States and other countries of the world: U. S. Geol. Survey Prof. Paper 492, 383 p.
Wasserburg, G. J., Kovach, R., Henyey, T., and Roy, R., 1966, Heat flow in the vicinity of the San Andreas fault [abs.]: Am. Geophys. Union Trans., v. 47, p. 181.
White, D. E., 1955, Violent mud-volcano eruption of Lake City Hot Springs, Northeastern California: Geol. Soc. America Bull., v. 66, p. 1109-1130.
_____ 1957a, Thermal waters of volcanic origin: Geol. Soc. America Bull., v. 68, p. 1637-1658.
_____ 1957b, Magmatic, connate, and metamorphic waters: Geol. Soc. America Bull., v. 68, p. 1659-1682.
_____ 1963, The Salton Sea geothermal brine, an ore-transporting fluid [abs.]: Mining Eng., v. 15, p. 60.
_____ 1965a, Geothermal energy: U. S. Geol. Survey Circular 519, 17 p.
_____ 1965b, Saline waters of sedimentary rocks, *in* Fluids in subsurface environments: Am. Assoc. Petroleum Geologists Symposium Mem. 4, p. 342-366.
_____ 1965c, Metal contents of some geothermal fluids: Symposium on problems of postmagnetic ore deposition, II, Prague, p. 432-443.
White, D. E., and Muffler, L. J. P., 1964, Metamorphism of upper Cenozoic sediments to greenschist mineral assemblages; Salton Sea geothermal area, California [abs.]: Geol. Soc. America Spec. Paper 82, p. 221-222.
White, D. E., Anderson, E. T., and Grubbs, D. K., 1963, Geothermal brine well: Mile-deep hole may tap ore-bearing magmatic water and rocks undergoing metamorphism: Science, v. 139, p. 919-922.
White, D. E., Hem, J. D., and Waring, G. A., 1963, Chemical composition of subsurface waters: U. S. Geol. Survey Prof. Paper 440-F, 67 p.